Time-dependent injection strategies for multilayer Hele-Shaw and porous media flows

Craig Gin
Department of Population Health and Pathobiology, North Carolina State University, Raleigh, North Carolina 27607, USA

Prabir Daripa
Department of Mathematics, Texas A&M University, College Station, Texas 77843, USA

(Received 11 August 2020; accepted 19 February 2021; published 5 March 2021)

We use linear stability analysis to demonstrate how to stabilize multilayer radial Hele-Shaw and porous media flows with a time-dependent injection rate. Sufficient conditions for an injection rate that maintains a stable flow are analytically derived for flows with an arbitrary number of fluid layers. We show numerically that the maximum injection rate for a stable flow decreases proportional to $t^{-1/3}$ for $t \gg 1$ regardless of the number of fluid layers. However, the constant of proportionality depends on the number of layers and increases at a rate that is proportional to the number of interfaces to the two-thirds power. Therefore, flows with more fluid layers can be stable with faster time-dependent injection rates than comparable flows with fewer fluid layers, even when the additional layers are very thin. We also show that for unstable flows, which may be required to inject a given amount of fluid in a fixed amount of time, an increasing injection rate is less unstable than a constant or decreasing injection rate, and that the inclusion of more fluid layers can overcome poor injection strategies.

DOI: 10.1103/PhysRevFluids.6.033901

I. INTRODUCTION

There are many applications in which one fluid displaces another fluid in a porous medium, including oil recovery, hydrology, filtration, and fixed bed regeneration in chemical processing. In the case that the displacing fluid is less viscous than the displaced fluid, the interface between the fluids is unstable and viscous fingering ensues. In some of the aforementioned applications, several fluids with favorable properties are used in succession to displace the resident fluid in the porous medium. An example of this is chemical enhanced oil recovery (EOR) in which various tertiary displacement processes are employed to contain this instability to a meaningful level before breakthrough (see Refs. [1–3]). Shah and Schechter [4] describe in detail many of the processes involved in Alkali-Surfactant-Polymer (ASP) flooding, a type of chemical EOR, that lead to improved oil recovery. Slobod and Lestz [5] experimentally studied the effect of two types of flooding processes on stabilization in a Hele-Shaw cell. The first flooding process involved the use of a sequence of polysolutions (polymer mixed with an aqueous phase) having different constant viscosities with stepwise jumps in viscosity at each of the fronts that are positive in the direction of displacement. The study resulted in significant stabilization of the fingering instability.

In what follows, we consider the case in which the injected fluids are all immiscible. In some EOR flooding schemes, it is possible that an aqueous phase-based liquid is displacing a different aqueous phase liquid. In such a case, a thin layer of spacer fluid of some nonaqueous phase liquid

(NAPL) between such miscible phases can be used to ensure immiscibility [6]. Alternatively, the injected fluid layers themselves can alternate between aqueous phases and NAPLs.

Viscous fingering in porous media flows [7] is often studied using the Hele-Shaw model in which there is a sharp interface between immiscible fluids. The influence of heterogeneity in porous media is nontrivial and is difficult to account for with the Hele-Shaw model. Therefore, the Hele-Shaw model is more directly relevant to homogeneous porous media. A linear stability analysis of viscous fingering within the Hele-Shaw model was performed by Saffman and Taylor [8]. They studied the case in which the fluid moves linearly and orthogonal to a planar interface. We refer to this flow configuration as rectilinear flow. An appropriate model for flow near an injection or production well is radial flow. The stability of radial Hele-Shaw flows was studied by Bataille [9] and Wilson [10] and was later developed further by Paterson [11].

There are several different strategies that have been used to control or minimize the viscous fingering instability. One class of techniques involves adjusting the geometry of the classical Hele-Shaw cell. An example is the tapered Hele-Shaw cell in which the plates are not parallel but instead there is a gradient in the gap thickness. The effects of the tapered cell on the instability of the interface has been studied analytically, numerically, and experimentally in the rectilinear [12–16] and radial [15,17–20] geometries. Other modifications to the classical Hele-Shaw cell that impact the stability include rotating the cell [21–24], using an elastic membrane in place of one of the rigid plates [25–29], and changing the gap width over time [30–32]. Another class of techniques used to control the interfacial instability is to alter the properties of the fluids. This includes the use of variable viscosity fluids [33–35], chemically reactive fluids [36] and non-Newtonian fluids [37,38].

In controlling the instability of Hele-Shaw and porous media flows, one of the simplest parameters to control is the rate at which fluid is injected. Thomé *et al.* [39] studied Hele-Shaw flow in a sector geometry to bridge the gap between rectilinear and radial flow. They showed that a self-similar finger can grow in the sector geometry with an injection rate proportional to $t^{-1/3}$. This was further studied in the sector geometry by Brener *et al.* [40], Ben Amar *et al.* [41], and Combescot and Ben Amar [42]. The $t^{-1/3}$ injection rate was studied numerically in the radial geometry by Li *et al.* [43]. They showed analytically that the wave number of the most unstable wave (and hence the number of fingers) can be made constant in time by using the $t^{-1/3}$ injection rate. Through numerical experiments, they demonstrated that the limiting shape of the interface is found to be independent of the initial conditions. Zheng *et al.* [31] studied a class of time-dependent control strategies of which the $t^{-1/3}$ injection rate is a special case. The validity of the $t^{-1/3}$ injection rate for producing self-similar solutions has also been explored numerically in the context of miscible flows [44] and a time-dependent gap width [20].

Another avenue of research involving time-dependent injection rates is attempting to minimize or completely suppress the viscous fingering instability. In the case of miscible flow in the quarter five-spot geometry, Chen and Meiburg [45] found that starting with a slow constant injection rate and then smoothly increasing the injection rate resulted in greater recovery (in the context of EOR) than a constant injection rate with the same average rate. Yuan and Azaiez [46] found that a piecewise constant injection scheme could reduce the fingering instability in comparison to a constant injection scheme for miscible flows in a rectilinear geometry. This came after Dias *et al.* [47] had shown that a similar strategy could reduce the size of fingers in the case of immiscible flow in a radial geometry. Also in the context of immiscible radial flow, Dias *et al.* [48] studied the optimal injection policy for a given average injection rate and found that a linearly increasing injection rate approximates the optimal injection rate. Huang and Chen [49] verified the success of a linearly increasing injection rate for a broader range of parameters than Ref. [48] and showed that these results do not hold for miscible flow. Going a step further than this is completely stabilizing the flow using a time-dependent injection rate. Beeson-Jones and Woods [50] found the maximum possible time-dependent injection rate for a stable radial Hele-Shaw flow.

Increasing the number of fluid layers can also be an effective means of controlling viscous fingering. This strategy is motivated by the various flooding schemes used in chemical EOR. However, there have been relatively few stability studies on flows with more than two fluid layers.

Of the existing studies, the majority are in the rectilinear geometry. Daripa [51] studied three-layer rectilinear Hele-Shaw flows and derive a formula for a critical value of the viscosity of the middle layer fluid that minimizes the bandwidth of unstable waves. Daripa also formulated the stability problem for rectilinear Hele-Shaw flows with an arbitrary number of fluid layers [52]. In that paper, the Rayleigh quotient and some inequalities are used to derive upper bounds on the growth rate of instabilities. Cardoso and Woods [53] studied three-layer flows in both the rectilinear and radial flow geometries. For radial flows, they considered flows in which the inner interface is stable and used the linear theory to predict the number of drops formed when the interfaces meet. Ward and White [54] performed experiments for three-layer radial flows in which a liquid composes the intermediate layer between two gases. Thus, in contrast to Ref. [53], the outer interface is stable. White and Ward [55] followed up this work by considering the same problem with a non-Newtonian fluid in the intermediate layer. Gin and Daripa [56] performed a linear stability analysis of multilayer (i.e., more than two-layer) radial flows in which all of the interfaces are unstable. They studied flows with an arbitrary number of fluid layers. Beeson-Jones and Woods [50] studied three-layer radial flow and used linear stability to find the optimal value of the viscosity of the intermediate fluid to inject fluid at the fastest rate possible while maintaining a stable flow. Recently, Anjos and Li [57] performed a weakly nonlinear analysis of three-layer radial flows. This was followed up by nonlinear simulations of three-layer radial flow by Zhao *et al.* [58].

With all the different types of control strategies described above, it is important to study the interplay between them. Some notable examples of studies that have looked at the interaction between multiple control strategies include Dias and Miranda [59], who studied radial flows in a tapered Hele-Shaw cell in which the gap width is time dependent, and Morrow *et al.* [20] who studied a wide variety of control strategies, including time-dependent injection, time-dependent gap width, and tapered and rotating Hele-Shaw cells. In the present paper, we consider the interplay between time-dependent injection strategies and the use of more than two fluid layers. To date, this has only been studied in a limited capacity. Time-dependent injection was considered for multilayer flow by Ward and White [54] and White and Ward [55]. These works were experimental and, as previously stated, involved three-layer flows in which only one interface was unstable. The only known analytical study of time-dependent injection for multilayer flow is Beeson-Jones and Woods [50]. Again, this work only considers three-layer flow and the only time-dependent control strategy considered is completely stabilizing the flow. Therefore, there is a need to study how time-dependent injection schemes impact flows with more than three layers and how these strategies change as additional fluids are added. Examining time-dependent injection strategies for flows with more than three layers is the main thrust of this paper. In what follows, we derive a dynamical system governing the linearized motion of interfaces for an arbitrary number of fluid layers. In contrast to the previous work that considers radial flows with an arbitrary number of fluid layers [56], the formulation in the present paper can be used to solve for the motion of each individual interface. We then study the maximum injection rate which results in a stable Hele-Shaw flow with an arbitrary number of interfaces. We provide analytically derived bounds on this injection rate and numerically investigate how it changes with the number of fluid layers. Additionally, we numerically investigate two different time-dependent injection strategies and demonstrate that a monotonically increasing injection rate is less unstable than a comparable constant or monotonically decreasing injection rate.

The paper is laid out as follows. In Sec. II, the stability problem is formulated for multilayer Hele-Shaw flows with an arbitrary number of fluid layers. The maximum time-dependent injection rate that stabilizes a multilayer flow is analyzed in Sec. III. We provide analytically derived bounds on this injection rate and investigate limiting cases. In Sec. IV, we numerically investigate how the maximum injection rate for a stable flow changes with the number of fluid layers. We also show numerically that the results of Ref. [48] about optimal injection strategies extend to multilayer flows and that multilayer flows can overcome even bad injection strategies. Concluding remarks are given in Sec. V.

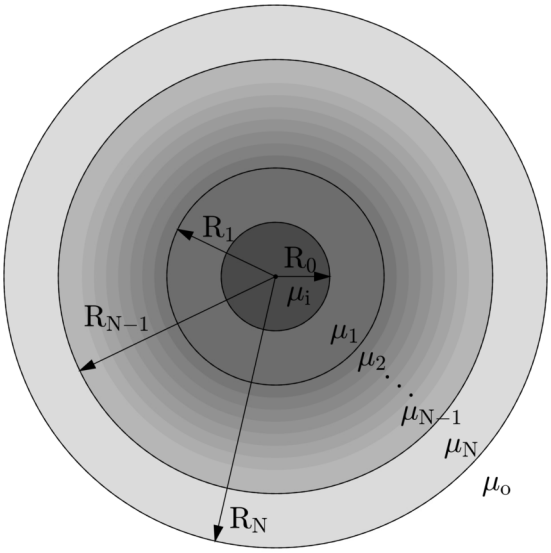

FIG. 1. The basic solution for (N + 2)-layer flow. The radius of the outermost interface is R_N.

II. PRELIMINARIES

Consider a radial source flow consisting of $(N + 2)$ regions of incompressible, immiscible fluid in a Hele-Shaw cell. By averaging across the gap, we may consider two-dimensional flow in polar coordinates, $\Omega := (r, \theta) = \mathbb{R}^2$. The least viscous fluid with viscosity μ_i is injected into the center of the cell at injection rate Q. The most viscous fluid, with viscosity μ_o, is the outermost fluid. There are N internal layers of fluid with viscosity μ_j for $j = 1, \ldots, N$ where $\mu_i < \mu_j < \mu_o$ for all j. The fluid flow is governed by the following equations:

$$\nabla \cdot \mathbf{u}_m = 0, \quad \nabla\, p_m = -\frac{\mu_m}{\kappa}\, \mathbf{u}_m, \quad \text{for } r \neq 0, \tag{1}$$

where $\kappa = b^2/12$, and b is the width of the gap of the Hele-Shaw cell. The governing equations hold within each fluid layer and the subscript $m = i, 1, 2, ..., N, o$ denotes the fluid region (where i denotes the innermost layer and o denotes the outermost layer). In what follows, we omit this subscript for quantities or equations that apply to all fluid layers and when it will not cause confusion to simplify the notation. The first equation, Eq. $(1)_1$, is the continuity equation for incompressible flow, and the second equation, Eq. $(1)_2$, is Darcy's law [60]. Initially, the fluids are separated by circular interfaces with radii $R = R_j(0)$, $j = 0, ..., N$, where $R_j(t)$ are the positions of the interfaces at time t, and T_j are the corresponding interfacial tensions. This setup is shown in Fig. 1.

The equations admit a simple basic solution in which all of the fluid moves outward radially with velocity $\mathbf{u} := (u_r, u_\theta) = (Q/(2\pi r), 0)$. The interfaces remain circular and move outward with velocity $Q/(2\pi R_j(t))$. The pressure, $p = p(r)$, may be obtained by integrating Eq. $(1)_2$.

We scale the variables using the characteristic length $R_N(0)$, the characteristic interfacial tension T_N, and the characteristic viscosity μ_o. The characteristic injection rate Q_{ref} is the injection rate at which a single interface at $R_N(0)$ with interfacial tension T_N and for which a fluid with viscosity μ_o is displaced by an inviscid fluid becomes unstable to a disturbance with wave number 2 (see Ref. [50]). Therefore,

$$Q_{\text{ref}} = \frac{12\pi\kappa T_N}{R_N(0)\mu_o}, \tag{2}$$

$$Q^* = \frac{Q}{Q_{\text{ref}}}, \tag{3}$$

$$r^* = \frac{r}{R_N(0)}, \tag{4}$$

$$\mu^* = \frac{\mu}{\mu_o}, \tag{5}$$

$$t^* = \frac{12\kappa T_N}{R_N^3(0)\mu_o}t, \tag{6}$$

$$\mathbf{u}^* = \frac{R_N^2(0)\mu_o}{12\kappa T_N}\mathbf{u}, \tag{7}$$

$$p^* = \frac{R_N(0)}{12T_N}p, \tag{8}$$

$$T^* = \frac{T}{T_N}. \tag{9}$$

In these dimensionless variables, Eqs. (1) become

$$\nabla^* \cdot \mathbf{u}^* = 0, \quad \nabla^* p^* = -\mu^* \mathbf{u}^*, \quad \text{for } r^* \neq 0, \tag{10}$$

and the velocity of the basic solution is $\mathbf{u}^* = (Q^*/(2r^*), 0)$. With a slight abuse of notation, we drop the stars below for convenience. We perturb the basic solution (u_r, u_θ, p) by $(\tilde{u}_r, \tilde{u}_\theta, \tilde{p})$. Since Eqs. (10) are linear, the disturbances satisfy the same equations. Therefore,

$$\frac{\partial \tilde{u}_r}{\partial r} + \frac{\tilde{u}_r}{r} + \frac{1}{r}\frac{\partial \tilde{u}_\theta}{\partial \theta} = 0, \quad \frac{\partial \tilde{p}}{\partial r} = -\mu \tilde{u}_r, \quad \frac{1}{r}\frac{\partial \tilde{p}}{\partial \theta} = -\mu \tilde{u}_\theta. \tag{11}$$

We use separation of variables and assume that the disturbances are of the form

$$(\tilde{u}_r, \tilde{u}_\theta, \tilde{p}) = (f(r), \tau(r), \psi(r))g(t)e^{in\theta}. \tag{12}$$

Using Eq. (12) in Eqs. (11) yields the following ordinary differential equation for $f(r)$:

$$(r^3 f'(r))' - (n^2 - 1)rf(r) = 0. \tag{13}$$

The above equation is exact since there has been no linearization in its derivation.

Next we derive the boundary conditions for this equation from linearization of the dynamic interfacial boundary conditions. Let the disturbance of the interface located at $R_j(t)$ be given by $A_n^j(t)e^{in\theta}$. The linearized kinematic interface conditions are given by

$$\frac{dA_n^j(t)}{dt} = f(R_j)g(t) - A_n^j(t)\frac{Q}{2R_j^2}. \tag{14}$$

The linearized dynamic interface condition (see Eq. (10) in Ref. [56]) at the innermost interface located at $R = R_0$ is

$$\begin{aligned}&\{f(R_0)(\mu_i - \mu_1) + R_0[\mu_i(f^-)'(R_0) - \mu_1(f^+)'(R_0)]\}g(t)\\ &= \left\{\frac{Qn^2}{2R_0^2}(\mu_1 - \mu_i) - \frac{T_0}{12}\frac{n^4 - n^2}{R_0^3}\right\}A_n^0(t).\end{aligned} \tag{15}$$

The linearized dynamic condition at the outermost interface located at $R = R_N$ is

$$\begin{aligned}&\{f(R_N)(\mu_N - 1) + R_N[\mu_N(f^-)'(R_N) - (f^+)'(R_N)]\}g(t)\\ &= \left\{\frac{Qn^2}{2R_N^2}(1 - \mu_N) - \frac{1}{12}\frac{n^4 - n^2}{R_N^3}\right\}A_n^N(t).\end{aligned} \tag{16}$$

For any intermediate interface at $R = R_j$, the dynamic condition is

$$\{f(R_j)(\mu_j - \mu_{j+1}) + R_j[\mu_j(f^-)'(R_j) - \mu_{j+1}(f^+)'(R_j)]\}g(t) = \left\{\frac{Qn^2}{2R_j^2}(\mu_{j+1} - \mu_j) - \frac{T_j}{12}\frac{n^4 - n^2}{R_j^3}\right\}A_n^j(t). \tag{17}$$

Note that the dynamic interfacial condition on a three-dimensional interface involves two curvatures. Here, this would mean including the curvature in the thin dimension in the dynamic interfacial condition. This curvature arises due to contact line effects. In what follows, we have neglected this curvature effect with the assumption that contact line effects on the stability results are insignificant. This is done in most stability analyses of Hele-Shaw flows. However, Homsy [61] has addressed how to modify the dynamic boundary condition for Hele-Shaw flows to account for contact line effects.

Using the fact that $f(r)$ is a solution to the differential Eq. (13), the dynamic interface condition Eq. (15) at the innermost interface becomes

$$\left\{\mu_i - \mu_1\frac{\left(\frac{R_0}{R_1}\right)^{2n} + 1}{\left(\frac{R_0}{R_1}\right)^{2n} - 1}\right\}f(R_0)g(t) + 2\mu_1\frac{\left(\frac{R_0}{R_1}\right)^{n-1}}{\left(\frac{R_0}{R_1}\right)^{2n} - 1}f(R_1)g(t) = F_0A_n^0(t), \tag{18}$$

where

$$F_0 = \frac{Qn}{2R_0^2}(\mu_1 - \mu_i) - \frac{T_0}{12}\frac{n^3 - n}{R_0^3}. \tag{19}$$

Similarly, the dynamic interface condition Eq. (16) for the outermost interface reduces to

$$\left\{1 - \mu_N\frac{\left(\frac{R_{N-1}}{R_N}\right)^{2n} + 1}{\left(\frac{R_{N-1}}{R_N}\right)^{2n} - 1}\right\}f(R_N)g(t) + 2\mu_N\frac{\left(\frac{R_{N-1}}{R_N}\right)^{n+1}}{\left(\frac{R_{N-1}}{R_N}\right)^{2n} - 1}f(R_{N-1})g(t) = F_NA_n^N(t), \tag{20}$$

where

$$F_N = \frac{Qn}{2R_N^2}(1 - \mu_N) - \frac{1}{12}\frac{n^3 - n}{R_N^3}, \tag{21}$$

and the dynamic interface conditions at the intermediate interfaces are

$$\left\{-\mu_j\frac{\left(\frac{R_{j-1}}{R_j}\right)^{2n} + 1}{\left(\frac{R_{j-1}}{R_j}\right)^{2n} - 1} - \mu_{j+1}\frac{\left(\frac{R_j}{R_{j+1}}\right)^{2n} + 1}{\left(\frac{R_j}{R_{j+1}}\right)^{2n} - 1}\right\}f(R_j)g(t) + 2\mu_j\frac{\left(\frac{R_{j-1}}{R_j}\right)^{n+1}}{\left(\frac{R_{j-1}}{R_j}\right)^{2n} - 1}f(R_{j-1})g(t) + 2\mu_{j+1}\frac{\left(\frac{R_j}{R_{j+1}}\right)^{n-1}}{\left(\frac{R_j}{R_{j+1}}\right)^{2n} - 1}f(R_{j+1})g(t) = F_jA_n^j(t), \tag{22}$$

where

$$F_j = \frac{Qn}{2R_j^2}(\mu_{j+1} - \mu_j) - \frac{T_j}{12}\frac{n^3 - n}{R_j^3}, \quad j = 1, \ldots, N-1. \tag{23}$$

Equations (18), (20), and (22) can be written as a system of equations of the form

$$\widetilde{\mathbf{M}}_N(t)\begin{pmatrix} f(R_0)g(t) \\ \vdots \\ f(R_N)g(t) \end{pmatrix} = \begin{pmatrix} F_0A_n^0(t) \\ \vdots \\ F_NA_n^N(t) \end{pmatrix},$$

where $\widetilde{\mathbf{M}}_N(t)$ is the $(N+1)\times(N+1)$ tridiagonal matrix with entries indexed by $i, j = 0, ...N$ given by

$$
\begin{aligned}
(\widetilde{\mathbf{M}}_N(t))_{00} &= \mu_i - \mu_1 \frac{\left(\frac{R_0}{R_1}\right)^{2n}+1}{\left(\frac{R_0}{R_1}\right)^{2n}-1}, \quad (\widetilde{\mathbf{M}}_N(t))_{01} = 2\mu_1 \frac{\left(\frac{R_0}{R_1}\right)^{n-1}}{\left(\frac{R_0}{R_1}\right)^{2n}-1} \\
(\widetilde{\mathbf{M}}_N(t))_{j,j-1} &= 2\mu_j \frac{\left(\frac{R_{j-1}}{R_j}\right)^{n+1}}{\left(\frac{R_{j-1}}{R_j}\right)^{2n}-1}, \quad (\widetilde{\mathbf{M}}_N(t))_{j,j} = -\mu_j \frac{\left(\frac{R_{j-1}}{R_j}\right)^{2n}+1}{\left(\frac{R_{j-1}}{R_j}\right)^{2n}-1} - \mu_{j+1} \frac{\left(\frac{R_j}{R_{j+1}}\right)^{2n}+1}{\left(\frac{R_j}{R_{j+1}}\right)^{2n}-1}, \\
(\widetilde{\mathbf{M}}_N(t))_{j,j+1} &= 2\mu_{j+1} \frac{\left(\frac{R_j}{R_{j+1}}\right)^{n-1}}{\left(\frac{R_j}{R_{j+1}}\right)^{2n}-1}, \quad (\widetilde{\mathbf{M}}_N(t))_{N,N-1} = 2\mu_N \frac{\left(\frac{R_{N-1}}{R_N}\right)^{n+1}}{\left(\frac{R_{N-1}}{R_N}\right)^{2n}-1}, \\
(\widetilde{\mathbf{M}}_N(t))_{N,N} &= 1 - \mu_N \frac{\left(\frac{R_{N-1}}{R_N}\right)^{2n}+1}{\left(\frac{R_{N-1}}{R_N}\right)^{2n}-1}.
\end{aligned} \tag{24}
$$

Combining this system of equations with the linearized kinematic interface conditions yields the dynamical system governing the evolution of interfacial disturbances for multilayer flows,

$$
\frac{d}{dt}\begin{pmatrix} A_n^0(t) \\ \vdots \\ A_n^N(t) \end{pmatrix} = \mathbf{M}_N(t)\begin{pmatrix} A_n^0(t) \\ \vdots \\ A_n^N(t) \end{pmatrix}, \tag{25}
$$

where

$$
\mathbf{M}_N(t) = \widetilde{\mathbf{M}}_N^{-1}(t)\begin{pmatrix} F_0 & \dots & 0 \\ \vdots & \ddots & \vdots \\ 0 & \dots & F_N \end{pmatrix} - \frac{Q}{2}\begin{pmatrix} \frac{1}{R_0^2} & \dots & 0 \\ \vdots & \ddots & \vdots \\ 0 & \dots & \frac{1}{R_N^2} \end{pmatrix}. \tag{26}
$$

For the particular case of $N = 1$ (i.e., three-layer flow), the matrix $\widetilde{\mathbf{M}}_1$ is a 2×2 matrix and can be easily inverted and plugged into Eq. (26) to obtain the matrix $\mathbf{M}_1(t)$ with entries indexed by $i, j = 0, 1$ given by

$$
\begin{aligned}
(\mathbf{M}_1(t))_{00} &= \frac{\left\{(1+\mu_1) - (1-\mu_1)\left(\frac{R_0}{R_1}\right)^{2n}\right\}F_0}{(\mu_1-\mu_i)(1-\mu_1)\left(\frac{R_0}{R_1}\right)^{2n} + (\mu_1+\mu_i)(1+\mu_1)} - \frac{Q}{2R_0^2}, \\
(\mathbf{M}_1(t))_{01} &= \frac{2\mu_1\left(\frac{R_0}{R_1}\right)^{n-1}F_1}{(\mu_1-\mu_i)(1-\mu_1)\left(\frac{R_0}{R_1}\right)^{2n} + (\mu_1+\mu_i)(1+\mu_1)}, \\
(\mathbf{M}_1(t))_{10} &= \frac{2\mu_1\left(\frac{R_0}{R_1}\right)^{n+1}F_0}{(\mu_1-\mu_i)(1-\mu_1)\left(\frac{R_0}{R_1}\right)^{2n} + (\mu_1+\mu_i)(1+\mu_1)}, \\
(\mathbf{M}_1(t))_{11} &= \frac{\left\{(\mu_1+\mu_i) + (\mu_1-\mu_i)\left(\frac{R_0}{R_1}\right)^{2n}\right\}F_1}{(\mu_1-\mu_i)(1-\mu_1)\left(\frac{R_0}{R_1}\right)^{2n} + (\mu_1+\mu_i)(1+\mu_1)} - \frac{Q}{2R_1^2}.
\end{aligned} \tag{27}
$$

Note that these entries are time dependent because the radii R_0 and R_1 are time dependent as well as possibly the injection rate Q. Hence the matrix $\mathbf{M}_1(t)$ is time dependent. Accounting for differences in notation and scaling, this matrix agrees with the one derived in Ref. [50].

III. MAXIMUM INJECTION RATE FOR A STABLE FLOW

Traditionally, the injection rate Q for a radial Hele-Shaw flow is taken to be constant. However, in the formulation above, the injection rate can be a function of time. There have been many studies that have explored the implications of using a strategically chosen time-dependent injection rate (see, for example, Refs. [31,43,48,50]). Almost all these studies are for two-layer flows with the exception of Ref. [50], which considers three-layer flows. In this section, we extend some of these results to flows with an arbitrary number of layers. In particular, we explore the time-dependent maximum injection rate for which a particular flow is stable. This is important for many applications including oil recovery, in which it is beneficial to stabilize the flow but it is also cost effective to inject as fast as possible.

A. Two-layer flow

To set the stage for time-dependent injection rates for flows with many fluid layers, we very briefly review a result that has already been established for two-layer flow in Ref. [50]. The maximum dimensionless injection rate for which the disturbance with wave number n is stable, which comes from setting the two-layer growth rate equal to zero and solving for the injection rate Q, is

$$Q_M(n) = \frac{1}{6R}\frac{n(n^2-1)}{n(1-\mu_i)-(1+\mu_i)}. \tag{28}$$

The maximum time-dependent injection rate for which the flow is stable, which we denote by Q_M, is found by taking the minimum of Eq. (28) over all values of n. It follows from inspecting Eq. (28) that $R \cdot Q_M$ will be constant over time. By conservation of mass, the injection rate $Q(t)$ is proportional to dR^2/dt. It then follows that $R \cdot dR^2/dt$ is constant or dt is proportional to $R^2 dR$. Upon integration, $R(t)$ is proportional to $t^{1/3}$. Hence, the injection rate Q_M is proportional to $t^{-1/3}$ since $R \cdot Q_M$ is constant.

B. Three-layer flow

We now wish to obtain a result analogous to Eq. (28) but for multilayer flows. The strategy described above for two-layer flow does not work in this case because Q cannot be isolated when setting the equation for the maximum growth rate for three-layer flow equal to zero. Additionally, the fact that $Q_M(n)$ is proportional to $t^{-1/3}$ relies on the fact that $R \cdot Q_M(n)$ is constant [i.e., all time-dependent terms can be moved to one side of Eq. (28)]. This cannot work for three-layer flows because the growth rates depend on the radii of both interfaces (R_0 and R_1). Therefore, instead of seeking an exact expression for $Q_M(n)$ we look for bounds that ensure stability of the flow.

We start by considering three-layer flow. By Gershgorin's circle theorem, both of the eigenvalues of $\mathbf{M}_1$ will have a negative real part if the terms on the diagonal are negative and greater in absolute value than the off-diagonal terms in the same row. This condition is satisfied if the following two inequalities hold:

$$\begin{aligned}
\frac{Q}{2R_0^2} &\geqslant \frac{\left\{(1+\mu_1)-(1-\mu_1)\left(\frac{R_0}{R_1}\right)^{2n}\right\}F_0 + 2\mu_1\left(\frac{R_0}{R_1}\right)^{n-1}F_1}{(\mu_1-\mu_i)(1-\mu_1)\left(\frac{R_0}{R_1}\right)^{2n}+(\mu_1+\mu_i)(1+\mu_1)}, \\
\frac{Q}{2R_1^2} &\geqslant \frac{\left\{(\mu_1+\mu_i)+(\mu_1-\mu_i)\left(\frac{R_0}{R_1}\right)^{2n}\right\}F_1 + 2\mu_1\left(\frac{R_0}{R_1}\right)^{n+1}F_0}{(\mu_1-\mu_i)(1-\mu_1)\left(\frac{R_0}{R_1}\right)^{2n}+(\mu_1+\mu_i)(1+\mu_1)}.
\end{aligned} \tag{29}$$

Recall from Eqs. (19) and (21) that both F_0 and F_1 depend on Q. By using Eqs. (19) and (21) in Eqs. (29) and solving for Q, the following condition on the injection rate is obtained which is

sufficient to ensure that the eigenvalues of $\mathbf{M}_1$ have negative real parts:

$$Q \leqslant \min\{G_0(n), G_1(n)\}, \tag{30}$$

where

$$G_0 = \frac{T_0}{6R_0}\frac{(n^3-n)D_0}{nD_1 - D_2}, \tag{31}$$

$$G_1 = \frac{1}{6R_1}\frac{(n^3-n)D_3}{nD_4 - D_2}, \tag{32}$$

$$D_0 = (1+\mu_1) + 2\mu_1 T_0^{-1}\left(\frac{R_0}{R_1}\right)^{n+2} - (1-\mu_1)\left(\frac{R_0}{R_1}\right)^{2n}, \tag{33}$$

$$D_1 = (1+\mu_1)(\mu_1-\mu_i) + 2\mu_1(1-\mu_1)\left(\frac{R_0}{R_1}\right)^{n+1} - (1-\mu_1)(\mu_1-\mu_i)\left(\frac{R_0}{R_1}\right)^{2n}, \tag{34}$$

$$D_2 = (1+\mu_1)(\mu_1+\mu_i) + (1-\mu_1)(\mu_1-\mu_i)\left(\frac{R_0}{R_1}\right)^{2n}, \tag{35}$$

$$D_3 = (\mu_1+\mu_i) + 2\mu_1 T_0\left(\frac{R_0}{R_1}\right)^{n-2} + (\mu_1-\mu_i)\left(\frac{R_0}{R_1}\right)^{2n}, \tag{36}$$

$$D_4 = (1-\mu_1)(\mu_1+\mu_i) + 2\mu_1(\mu_1-\mu_i)\left(\frac{R_0}{R_1}\right)^{n-1} + (1-\mu_1)(\mu_1-\mu_i)\left(\frac{R_0}{R_1}\right)^{2n}. \tag{37}$$

Therefore, the maximum injection rate for which a disturbance with wave number n is stable, $Q_M(n)$, is bounded below by the right-hand side of Eq. (30):

$$Q_M(n) \geqslant \min\{G_0(n), G_1(n)\}. \tag{38}$$

Considering all wave numbers, the maximum injection rate, Q_M, for which the flow is stable satisfies

$$Q_M \geqslant \min_{n\in\mathbb{N}}\{\min\{G_0(n), G_1(n)\}\}. \tag{39}$$

Note that the only terms in the expressions for G_0 and G_1 that are time dependent are R_0 and R_1. As time increases, the interfaces come closer to each other and $R_0/R_1 \to 1$ as $t \to \infty$. Therefore, from Eqs. (31) and (32), $G_0 \propto 1/R_0$ and $G_1 \propto 1/R_1$ as $t \to \infty$. This is precisely the relationship between Q and R in Eq. (28). Therefore, if the injection rate is chosen such that $Q = G_0$ or $Q = G_1$ then $Q \propto t^{-1/3}$ for $t \gg 1$.

Limiting cases

We now investigate the condition Eq. (30) in the limit when the intermediate layer is very thin ($R_0/R_1 \to 1$). Note that as fluid is injected for any three-layer Hele-Shaw flow, the average distance between the interfaces, $R_1 - R_0$, decreases with time. Therefore, even if the interfaces are initially far apart, the intermediate layer will eventually become thin. In the limit as $R_0/R_1 \to 1$, Eq. (31) becomes

$$\lim_{\frac{R_0}{R_1}\to 1} G_0(n) = \frac{1}{6R_0}\frac{(n^3-n)(T_0+1)}{n(1-\mu_i)-(1+\mu_i)}. \tag{40}$$

Likewise,

$$\lim_{\frac{R_0}{R_1}\to 1} G_1(n) = \frac{1}{6R_1}\frac{(n^3-n)(T_0+1)}{n(1-\mu_i)-(1+\mu_i)}. \tag{41}$$

Since we are considering the limit as $R_0/R_1 \to 1$, it is also true that $R_0 \to R_1$. If we denote $R := R_1$, then

$$\lim_{\frac{R_0}{R_1}\to 1} G_0(n) = \lim_{\frac{R_0}{R_1}\to 1} G_1(n) = \frac{1}{6R}\frac{(n^3-n)(T_0+1)}{n(1-\mu_i)-(1+\mu_i)}$$

and the condition Eq. (30) becomes

$$Q \leqslant \frac{1}{6R}\frac{(n^3-n)(T_0+1)}{n(1-\mu_i)-(1+\mu_i)}. \tag{42}$$

After some algebraic manipulation, this condition becomes

$$\frac{Qn}{2R^2}\frac{1-\mu_i}{1+\mu_i} - \frac{Q}{2R^2} - \frac{(T_0+1)}{1+\mu_i}\frac{(n^3-n)}{12R^3} \leqslant 0. \tag{43}$$

The term on the left-hand side is precisely the two-layer growth rate for a single interface with interfacial tension $T_0 + 1$ (in dimensional variables this is $T_0 + T_1$, the sum of the interfacial tensions of the two interfaces). This is the same thin-layer limit that was found for the exact three-layer growth rate in Ref. [56]. The thin-layer limit can also be inferred from physical considerations. The jump in pressure across the two interfaces in the thin layer limit is the sum of the pressure jumps across each of the interfaces since the intermediate layer fluid is nonexistent. This is also reflected in Eq. (43) due to the absence of the viscosity μ_1 of the intermediate layer fluid. This explains, in combination with Laplace's law of surface tension, that the effective interfacial tension must be the sum of the interfacial tensions of two interfaces.

Using a similar analysis of the thick-layer limit ($R_0 \ll R_1$) for $n > 2$, a disturbance with wave number n is stable if the injection rate Q is such that

$$\frac{Qn}{2R_0^2}\frac{\mu_1-\mu_i}{\mu_1+\mu_i} - \frac{Q}{2R_0^2} - \frac{T_0}{\mu_1+\mu_i}\frac{(n^3-n)}{12R_0^3} \leqslant 0 \tag{44}$$

and

$$\frac{Qn}{2R_1^2}\frac{1-\mu_1}{1+\mu_1} - \frac{Q}{2R_1^2} - \frac{1}{1+\mu_1}\frac{(n^3-n)}{12R_1^3} \leqslant 0. \tag{45}$$

Equation (44) is the condition that the inner interface is stable according to its two-layer growth rate, and Eq. (45) is the condition that the outer interface is stable according to its two-layer growth rate. Therefore, as expected, in the limit of a thick intermediate layer the interfaces are decoupled and the flow is stable if each interface is individually stable.

C. Multilayer flow

We now find sufficient conditions on the injection rate to stabilize a flow with an arbitrary number of fluid layers. The approach used for three-layer flows in Sec. III B which uses Gershgorin's circle theorem can be adapted to flows with four or more layers by calculating the corresponding matrix $\mathbf{M}_N$. However, to avoid inverting an $(N+1)\times(N+1)$ matrix, we adopt a different approach. In Ref. [56, p. 22], upper bounds are found on the real part of the growth rate for flows with N internal layers. This upper bound is the maximum of $N+1$ expressions, each of which has terms that pertain to the parameter values at one of the interfaces. From examining the upper bound, it can be seen that a disturbance with wave number n will be stable if $E_j \leqslant 0$ for $j = 0, 1, ..., N$. Using a dimensionless version of the upper bounds in Ref. [56], the relationship between E_j and F_j [see Eqs. (19), (21), and (23)] is

$$E_0 = nR_0^2F_0 - \frac{Qn}{2}\mu_i, \quad E_j = nR_j^2F_j, \quad \text{for } j = 1, ..., N-1, \quad E_N = nR_N^2F_N - \frac{Qn}{2}. \tag{46}$$

$E_j \leqslant 0$ for all j if

$$Q \leqslant \min\left\{\frac{1}{6R_0}\frac{T_0 n(n^2-1)}{n(\mu_1-\mu_i)-\mu_i}, \min_{j=1,\ldots,N-1}\frac{1}{6R_j}\frac{T_j(n^2-1)}{\mu_{j+1}-\mu_j}, \frac{1}{6R_N}\frac{n(n^2-1)}{n(1-\mu_N)-1}\right\}. \tag{47}$$

Therefore, a lower bound on the maximum stable injection rate Q_M is given by

$$Q_M \geqslant \min_{n\in\mathbb{N}}\left\{\min\left\{\frac{1}{6R_0}\frac{T_0 n(n^2-1)}{n(\mu_1-\mu_i)-\mu_i}, \min_{j=1,\ldots,N-1}\frac{1}{6R_j}\frac{T_j(n^2-1)}{\mu_{j+1}-\mu_j}, \frac{1}{6R_N}\frac{n(n^2-1)}{n(1-\mu_N)-1}\right\}\right\}. \tag{48}$$

Notice the similarity between the terms in Eq. (48) and the expression for two-layer flows given by Eq. (28).

The above approach can be used to obtain a bound on a stable injection rate for three-layer flows. However, the approach taken in Sec. III B using Gershgorin's circle theorem generally produces sharper bounds. This is because the effects of the interfaces have been decoupled in Eq. (48). Because the motion of the interfaces is inherently coupled, any bound that decouples them will not be a sharp bound.

IV. NUMERICAL RESULTS

In this section, we first numerically explore the maximum injection rate for a stable flow. Then we consider injection strategies that reduce instabilities for a given average injection rate by numerically integrating the dynamical system Eq. (25) to compute the motion of the interfaces within the linear theory and calculating the growth rates of interfacial disturbances. This system has a large parameter space. The parameters involved in the problem include the viscosities of each fluid, the interfacial tension of each interface, the injection rate, the initial positions of the interfaces, and the amplitude and wave numbers of the initial perturbations of the interfaces. In this paper, we focus on the injection rate. We have tested many values for the other parameters and have chosen values that exhibit behavior that is typical across parameter space. The values of the parameters are given in the various figure captions below.

All time stepping is performed using the Dormand-Prince method via MATLAB's `ode45`, and the maximum injection rate for a stable flow is found by using MATLAB's built-in `fzero` command to solve for the value of Q for which the maximum growth rate is zero.

A. Maximum injection rate for a stable flow

In this section, we investigate the maximum value of the injection rate that results in a stable flow, which is denoted Q_M. This was studied analytically in Sec. III. For two-layer radial flow, the maximum stable injection rate for a given wave number n and radius R of the circular interface is given exactly by the expression Eq. (28). Q_M is found by taking the minimum value over all integer wave numbers.

For flows with three or more layers, a lower bound on Q_M is calculated by minimizing the expression Eq. (39) or (48) over all integer values of n and with the initial positions of the interfaces $R_j(0)$. Then the interfacial positions $R_j(\Delta t)$ at the next time step Δt are calculated using this injection rate and the process is repeated. To find Q_M exactly for three-layer flow (see Fig. 2), an additional calculation is needed. There is no analytical expression for the maximum stable injection rate for given values of n, R_0, and R_1 analogous to Eq. (28). Therefore, we use the expression for $\sigma^+(t)$ given in Ref. [56]. A root-finding method is used to find the value of Q such that $\sigma^+(t) = 0$. A similar procedure is employed for flows with more than three layers, but the maximum growth rate is calculated numerically from the matrix $\mathbf{M}_n(t)$ in Eq. (26).

The maximum injection rate for which a certain two-layer flow is stable is given by the solid line in Fig. 2. As a comparison, the maximum stable injection rate is calculated for a three-layer flow in which the outer interface starts in the same position as the interface for two-layer flow, the viscosity of the inner and outer layers are the same as the two-layer flow, and the intermediate layer has a

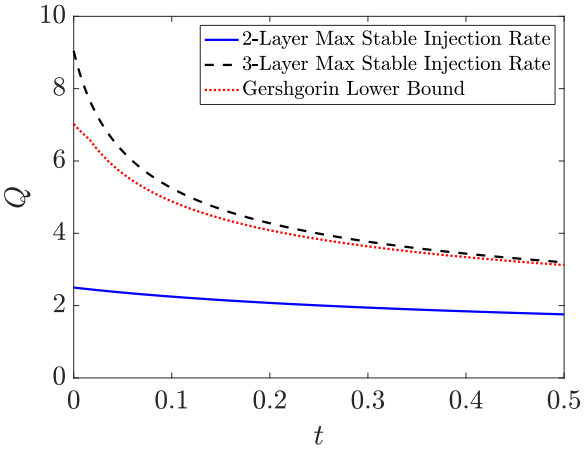

FIG. 2. Plots of the maximum stable injection rate versus time for two-layer flow (solid line) and three-layer flow (dashed line) as well as the lower bound for stabilization derived from Gershgorin's circle theorem and given by Eq. (39) (dotted line). The values of the parameters are $\mu_i = 0.2$, $\mu_o = 1$, $T = 1$, $R(0) = 1$ for two-layer flow and $\mu_i = 0.2$, $\mu_1 = 0.6$, $\mu_o = 1$, $T_0 = T_1 = 1$, $R_0(0) = 0.8$, $R_1(0) = 1$ for three-layer flow.

viscosity which is greater than the inner layer and smaller than the outer layer. This is the dashed line in Fig. 2. Note that the three-layer flow is stable for a much larger injection rate due to the fact that the viscosity jumps at the interfaces are smaller. Also included in Fig. 2 is the lower bound on the maximum stable injection rate given in Eq. (39). This is the dotted line in Fig. 2. Note that for these particular values of the parameters, this bound, while not strict, allows for a significant increase in the injection rate over two-layer flow.

In oil recovery applications, it is often expensive to include a more viscous intermediate fluid instead of just using water to displace oil. Therefore, it would be economically advantageous if a minimal amount of fluid could be used in the intermediate layer of a three-layer flow if it still allows the flow to be stabilized at a faster injection rate. This behavior is investigated in Fig. 3. The solid

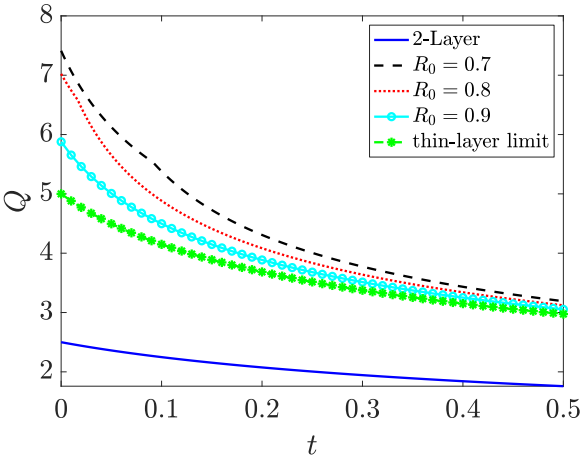

FIG. 3. Plots of the maximum stable injection rate versus time for two-layer flow (solid line) and three-layer flow (dashed line) as well as the lower bound Eq. (39) for three values of R_0. The values of the parameters are $\mu_i = 0.2$, $\mu_o = 1$, $T = 1$, $R(0) = 1$ for two-layer flow and $\mu_i = 0.2$, $\mu_1 = 0.6$, $\mu_o = 1$, $T_0 = T_1 = 1$, $R_0(0) = 0.7, 0.8, 0.9$, $R_1(0) = 1$ for three-layer flow.

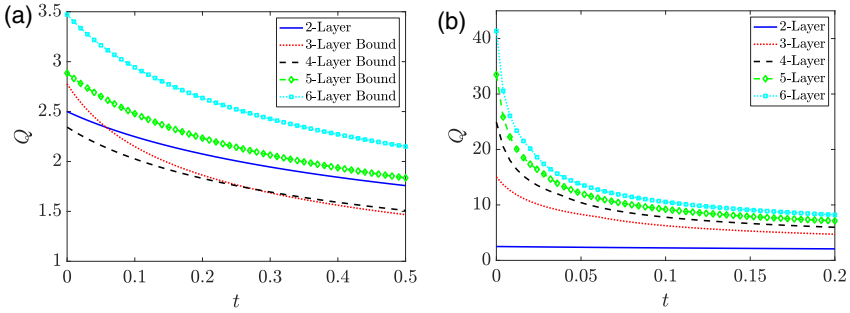

FIG. 4. Plots of the maximum stable injection rate versus time for flows with two through six fluid layers. Plot (a) uses the lower bound given by Eq. (48) for flows with three or more layers while plot (b) shows the actual maximum stable injection rate. The values of the parameters are $\mu_i = 0.2$, $\mu_o = 1$, $T_j = 1$ for all j, $R_0(0) = 0.6$, and $R_N(0) = 1$. The interfaces are equally spaced at time $t = 0$ in all cases and the viscous jumps are the same at all interfaces.

line is the maximum stable injection rate for two-layer flow using the same parameters as in Fig. 2. This flow is compared with three-layer flows for which the inner interface is initially at $R_0(0) = 0.7, 0.8, 0.9$. Notice that as the middle layer becomes thinner, the maximum stable injection rate decreases. Recall from Sec. III B 1 that in the limit of an infinitely thin middle layer, the flow will be stable when Q satisfies Eq. (42). The injection rate obtained by taking the minimum value of Q over all n from Eq. (42) is also plotted against time as the thin-layer limit in Fig. 3. Equation (42) is the same condition as the stable injection rate for two-layer flow but with effective interfacial tension $T_0 + T_1$. Therefore, a three-layer flow with a very thin intermediate layer will be stable for faster injection rates than the corresponding two-layer flow as long as the sum of the interfacial tensions in the three-layer flow is greater than the interfacial tension of the two-layer flow. Note that this does *not* depend on the viscosity of the intermediate fluid. The fact that the middle layer can be very thin leads to the conclusion that the use of a thin layer of spacer fluid with desirable properties can be a viable injection strategy.

We next compare estimates of the maximum stable injection rates using the lower bound Eq. (48) to explore how the bound changes as the number of layers increases. Recall that Eq. (48) gives a lower bound on the maximum stable injection rate for a flow with $(N + 2)$ layers (or N internal layers). This bound was computed for flows with three, four, five, and six layers and plotted in Fig. 4(a). For comparison, the maximum injection rate which results in a stable flow is plotted for two-layer flow [see Eq. (28)]. For all flows with more than one interface, the innermost interface has an initial position of $R_0(0) = 0.6$ and the other interfaces are evenly spaced at time $t = 0$. For all flows, the innermost fluid has a viscosity of $\mu_i = 0.2$, the outermost fluid has a viscosity of $\mu_o = 1$, and the viscosities of all intermediate layers are chosen so that the viscous jump at each interface is the same. All interfaces have the same interfacial tension. In general, the addition of more fluid layers increases the lower bound on the maximum stable injection rate. Intuitively, this is because the jumps at the interfaces are smaller when there are more layers of fluid. The one exception is three-layer flow which has a larger lower bound than four-layer flow for short time. This is due to the fact that for three-layer flow, the lower bound on the maximum stable injection rate only includes the first and last terms of Eq. (48), which has a different structure than the intermediate terms. For flows with four or more layers and these parameter values, the intermediate terms produce the minima.

In addition to considering approximations to the maximum stable injection rate from lower bounds as discussed above, we also numerically compute the exact maximum stable injection rate for multilayer flows. For these computations, a root finding algorithm is used to find the value of Q that results in the maximum eigenvalue of the matrix $\mathbf{M}_N$ [defined in Eq. (26)] being zero.

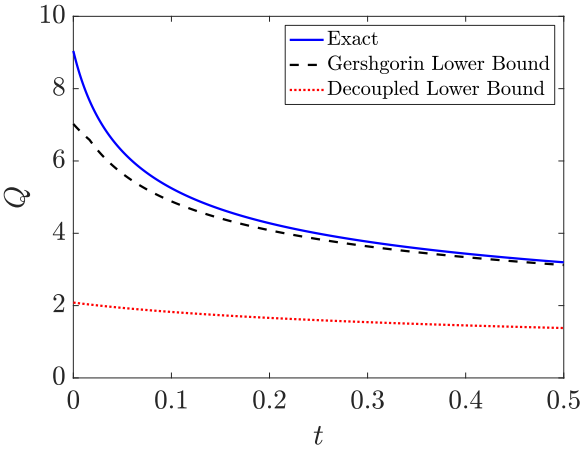

FIG. 5. Plot of the maximum stable injection rate versus time for three-layer flow (solid line) as well as the lower bound derived from Gershgorin's circle theorem [see Eq. (39)] and the decoupled lower bound [see Eq. (48)]. The values of the parameters are $\mu_i = 0.2$, $\mu_1 = 0.6$, $\mu_o = 1$, $T_0 = T_1 = 1$, $R_0(0) = 0.8$, $R_1(0) = 1$.

Figure 4(b) shows the maximum stable injection rates for flows with two, three, four, five, and six layers. The parameters used are the same as in Fig. 4(a). A comparison of Figs. 4(a) and 4(b) shows that the increase in the maximum stable injection rate from using additional layers of fluid is much greater than what is suggested by the lower bounds. This is especially true for short times. For example, for these values of the parameters the maximum stable injection rate at time $t = 0$ is more than 16 times greater for six-layer flow than it is for two-layer flow.

A comparison of Figs. 4(a) and 4(b) shows that the lower bounds given by Eq. (48) are crude. There is the potential to find analytical bounds which are sharper. In particular, the three-layer lower bound Eq. (39) found using Gershgorin's circle theorem gives a sharper bound than Eq. (48). One reason that the bound given by Eq. (39) is better is because the interfaces remain coupled whereas in the bounds given by Eq. (48) the interfaces have been decoupled. A bound for which the interfaces are coupled has the ability to account for interactions between the interfaces and therefore has the potential to be a sharper bound. Fig. 5 shows a comparison of the two bounds. The solid curve shows the exact value of the maximum stable injection rate for the same three-layer flow considered in Fig. 2. The dashed line is the lower bound given by Eq. (39) and the dotted line is the lower bound given by Eq. (48). The difference between the two bounds is stark.

Recall from Sec. III A that Beeson-Jones and Woods [50] showed that for two-layer flow (i.e., single interface), the maximum stable injection rate scales like $t^{-1/3}$ for $t \gg 1$. This also holds true for flows with multiple interfaces. For flows with 1 through 30 interfaces, we calculated the maximum stable injection rate from $t = 0$ to $t = 100$. For a subsample of these cases, the maximum stable injection rates are shown on a log-log scale in Fig. 6(a). As in Fig. 4(b), the initial position of the innermost interface is $R = 0.6$ and the initial position of the outermost interface is $R = 1$. The interfaces are equally spaced and the viscous jumps at the interfaces are all the same with $\mu_i = 0.2$ and $\mu_o = 1$. The interfacial tension is 1 for every interface. Note that after an initial period of time, all curves are linear with the same slope. For each curve, we fit an exponential function of the form $Q(t) = Ct^\alpha$ for $t \geqslant 10$. In all cases, the exponent of the best fit exponential function is approximately $\alpha = -1/3$, which matches with the analytically obtained scaling law for the single interface case. However, the constant C increases with the number of interfaces. The values of C are plotted versus the number of interfaces on a log-log scale in Fig. 6(b). The line of best fit through the points is shown in the figure and has slope 2/3. Therefore, if N_I is the number of interfaces, $C \propto N_I^{2/3}$. Thus $Q(t) \propto N_I^{2/3} t^{-1/3}$ for $t \geqslant 10$.

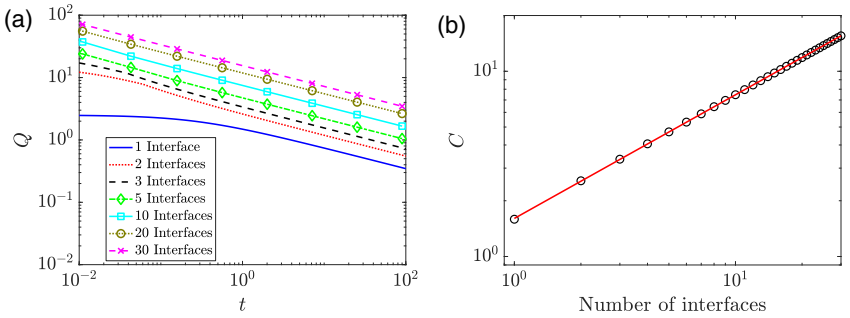

FIG. 6. Plot (a) is the maximum stable injection rate versus time for several different numbers of interfaces on a log-log scale. Each curve is of the form $Q(t) = Ct^{-1/3}$ for $t \gg 1$. Plot (b) shows C versus the number of interfaces on a log-log scale. The values of the parameters are $\mu_i = 0.2$, $\mu_o = 1$, $T_j = 1$ for all j, $R_0(0) = 0.6$, and $R_N(0) = 1$. The interfaces are equally spaced at time $t = 0$ in all cases and the viscous jumps are the same at all interfaces.

This relationship between C and N_I can be understood in the following way. First, notice that the maximum stable injection rate for flow with a single interface is independent of the interfacial tension T [see Eq. (28)]. However, the interfacial tension is part of both the characteristic injection rate and the characteristic timescale. The dimensionless injection rate Q^* is proportional to $1/T$ and the dimensionless time t^* is proportional to T. Therefore, since $Q^*(t^*) \propto (t^*)^{-1/3}$,

$$\frac{Q(t)}{T} \propto (Tt)^{-1/3} \Rightarrow Q(t) \propto T^{2/3} t^{-1/3}.$$

Recall from Sec. III B 1 that when there are two interfaces, they will eventually be very close together. In that limit, the maximum stable injection rate reduces to a term that is identical to a single interface maximum stable injection rate but with interfacial tension equal to the sum of the interfacial tensions of the two interfaces. Therefore, if both interfaces have the same interfacial tension, the maximum stable injection rate with two interfaces will be greater than the comparable single interface flow by a factor of $2^{2/3}$. For N_I interfaces, the long-time behavior is the same as the single interface case where the single interface has interfacial tension equal to the sum of the N_I interfacial tensions. Therefore, if all of the interfaces have the same interfacial tension we would expect that $Q(t) \propto N_I^{2/3}$ which agrees very well with the results of Fig. 6(a). We further verified this by looking at the maximum stable injection rate for $t \gg 1$ for flows with different numbers of interfaces, but where the sum of the interfacial tensions remained constant. In that case, the maximum stable injection rate converged to $Ct^{-1/3}$ for the same constant C for any number of interfaces because the thin-layer limits are all the same.

In summary, the injection rate for a stable flow increases at a rate proportional to the number of interfaces to the two-thirds power at large time $t \gg 1$. However, at earlier times the number of interfaces can increase the maximum stable injection rate by a much greater amount.

B. Optimizing stability for a fixed mean injection rate

In the previous section, we considered the maximum injection rate for a fully stable flow. However, in practical situations there may be some time constraint that does not allow for a slow enough injection rate to fully stabilize the flow. Another approach to the problem is to consider the case in which a certain amount of fluid needs to be injected in a fixed amount of time. The question is which time-dependent injection rate $Q(t)$ will have the smallest growth rate of instabilities and minimize the effects of viscous fingering. It may appear from the previous section that a *decreasing* injection rate of the form $Q(t) \propto t^{-1/3}$ would be optimal. However, Dias *et al.* [48] showed that for a single interface, the optimal injection rate is approximated by an injection profile which

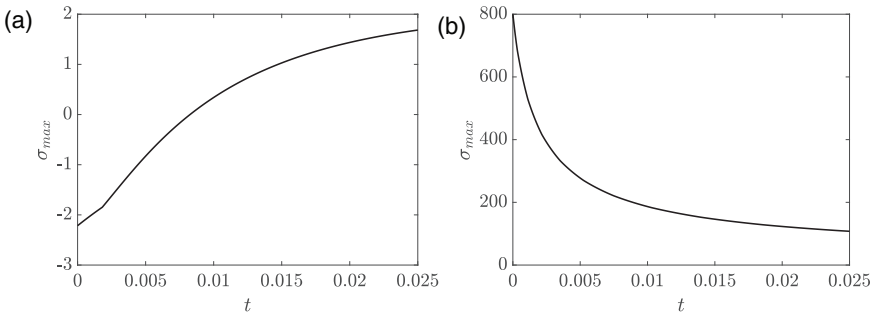

FIG. 7. The maximum growth rate $\sigma_{\max}$ versus time for two-interface flows with (a) a relatively low constant injection rate $Q = 15$, and (b) a relatively high constant injection rate $Q = 200$. The values of the other parameters are $\mu_i = 0.2$, $\mu_1 = 0.6$, $\mu_o = 1$, $T_0 = T_1 = 1$, $R_0(0) = 0.5$, and $R_N(0) = 1$.

increases linearly with t. We propose that this strategy is also effective for multiinterface flows for the following intuitive reasoning. Figure 7 shows the maximum growth rate $\sigma_{\max}$ for two flows that both have two interfaces and share the same parameters. The only difference is that the flow represented by Fig. 7(a) has a low constant injection rate $Q = 15$ for which the flow is initially stable and near the maximum stable injection rate during the duration of time that is plotted, and the flow represented by Fig. 7(b) has a high constant injection rate $Q = 200$ which is unstable for all time. Note that the slow flow in Fig. 7(a) has a maximum growth rate that increases with time while the fast flow in Fig. 7(b) has a maximum growth rate that decreases with time. Therefore, from Fig. 7(a) it makes sense that finding the maximum stable injection rate, which corresponds to enforcing $\sigma_{\max} = 0$, results in a decreasing injection rate. Namely, a slow flow with constant injection rate would become unstable over time, as in Fig. 7(a), and therefore a decrease in injection rate is required to maintain stability. However, Fig. 7(b) shows that for an unstable flow, injecting more quickly at the beginning would lead to instabilities growing very quickly initially. Therefore, it makes sense to inject more slowly at the beginning and gradually increase the injection rate in order avoid the initial behavior of Fig. 7(b).

We now demonstrate the effect of a variable injection rate on the motion of the interfaces according to the linear theory. In all of the results that follow, the parameters are chosen so that the jump in viscosity is the same across each interface and the unperturbed interfaces are initially evenly spaced. Figure 8(a) shows the results for a three-layer flow with a constant injection rate in which the interfaces are initially disturbed with white noise. The top plot shows the maximum growth rate over time (solid blue curve) and the injection rate (dashed red curve). The bottom plot shows the positions of the interfaces according to the linear theory at the beginning time $t = 0$ (solid blue curves), an intermediate time $t = 0.0125$ (dashed red curves), and at the final time $t = 0.025$ (dotted magenta curves). Figure 8(b) shows the results for a three-layer flow with the same parameters except that the injection rate is linearly increasing, but with the same average injection rate as the constant injection flow in Fig. 8(a). Notice that the maximum growth rate of disturbances for the linearly increasing injection rate is less than that of the constant injection rate and therefore the interfaces at the final time have a smaller disturbance. This effect is even stronger if more fluid layers are added. A comparable four-layer flow is shown in Fig. 8(c). The injection rate for this four-layer flow is linearly increasing and the flow is even less unstable than the three-layer flow with linearly increasing injection rate. Although not shown, the maximum growth rate is even smaller if more fluid layers are added.

An interesting feature of Fig. 8(b) is that the curve which represents the maximum growth rate $\sigma_{\max}$ versus time is not a smooth curve. This is because $\sigma_{\max}(t)$ is the maximum growth rate over all integer values of the wave number n at time t. The curve has a discontinuous derivative with respect to time when the wave number of the most unstable wave, which we denote $n_{\max}$, changes.

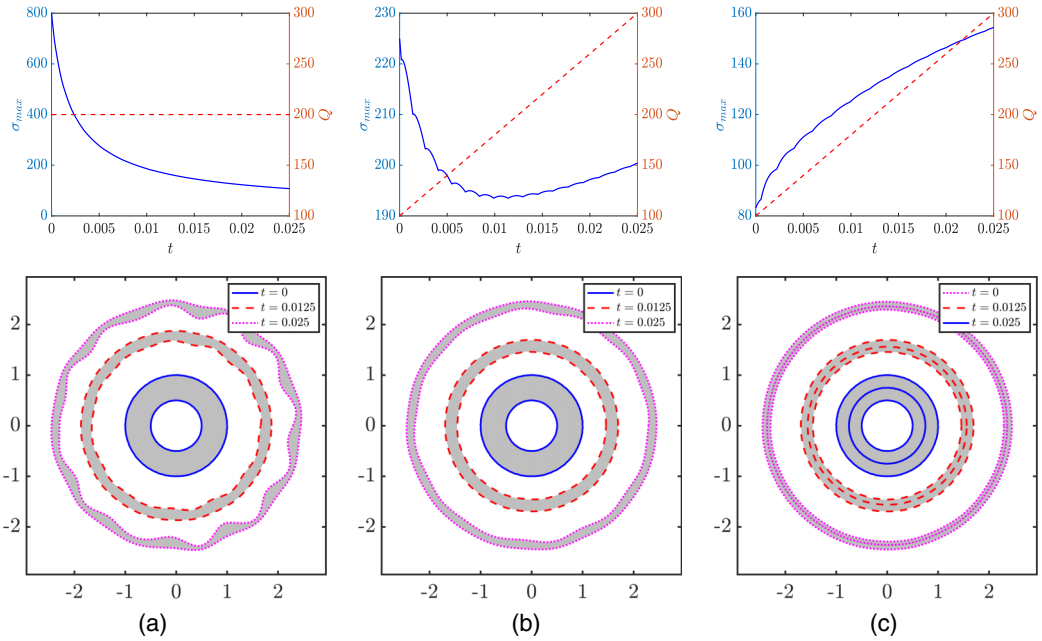

FIG. 8. The top row shows the maximum growth rate $\sigma_{\max}$ versus time and the injection rate Q versus time, and the bottom row shows the positions of the interfaces at the beginning, middle, and end times for (a) a constant injection rate with two interfaces, (b) a linearly increasing injection rate with two interfaces, and (c) a linearly increasing injection rate with three interfaces. The values of the parameters are $\mu_i = 0.2$, $\mu_o = 1$, $T_0 = T_1 = 1$, $R_0(0) = 0.5$, and $R_N(0) = 1$.

Figure 9 shows $n_{\max}$ versus time. The times that $n_{\max}$ changes correspond to the places where $\sigma_{\max}$ has a jump in its derivative.

The effectiveness of controlling the viscous fingering instability by adding additional fluid layers becomes evident when considering a suboptimal injection strategy. Figure 10 shows results that are

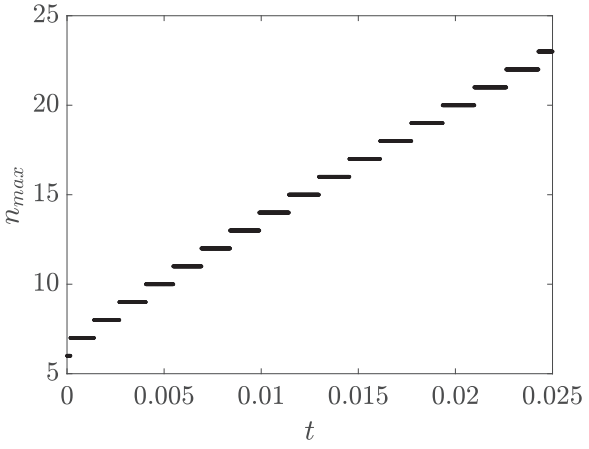

FIG. 9. Plot of the wave number $n_{\max}$ of the most unstable wave versus time for three-layer flow with a linearly increasing injection rate. The values of the parameters are the same as Fig. 8(b) [$\mu_i = 0.2$, $\mu_1 = 0.6$, $\mu_o = 1$, $T_0 = T_1 = 1$, $R_0(0) = 0.5$, $R_1(0) = 1$].

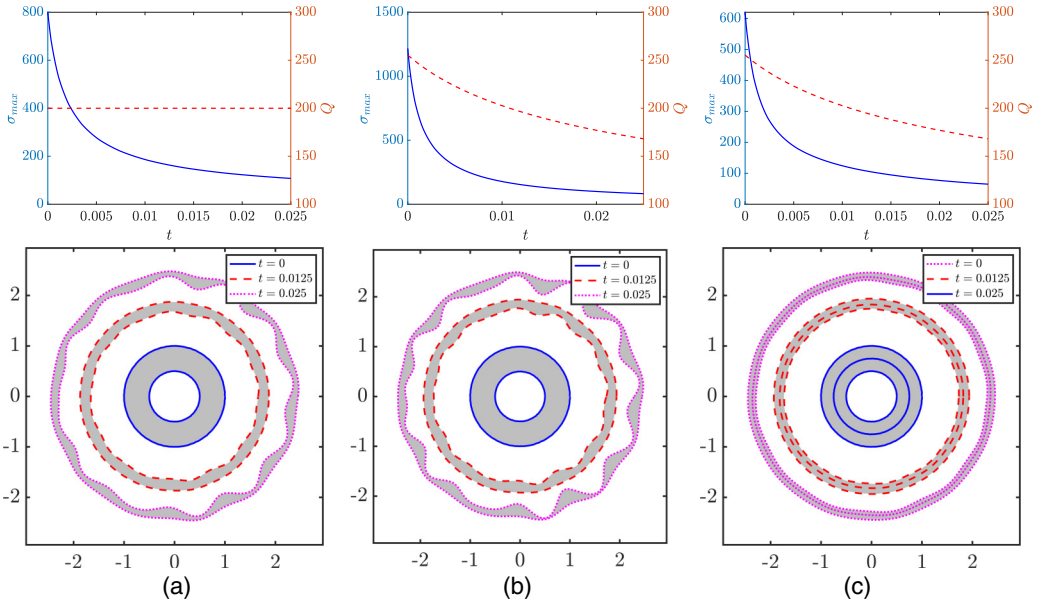

FIG. 10. The top row shows the maximum growth rate $\sigma_{\max}$ versus time and the injection rate Q versus time, and the bottom row shows the positions of the interfaces at the beginning, middle, and end times for (a) a constant injection rate with two interfaces, (b) a decreasing injection rate with two interfaces, and (c) a decreasing injection rate with three interfaces. The values of the parameters are $\mu_i = 0.2$, $\mu_o = 1$, $T_0 = T_1 = 1$, $R_0(0) = 0.5$, and $R_N(0) = 1$.

the same as those in Fig. 8 except that the variable injection strategies use a decreasing injection rate proportional to $t^{-1/3}$. Figure 10(a) is the same constant injection flow that is shown in Fig. 8(a). We repeat it for convenience. Figure 10(b) is a three-layer flow with a decreasing injection rate chosen so that the average injection rate is the same as the constant injection flow. Notice that in this case the variable injection rate causes the maximum growth rate to increase and the disturbances of the interfaces at later times are larger than the comparable constant injection flow. The decreasing injection rate is clearly a bad strategy. However, the addition of more fluid layers can help stabilize the flow, even with this bad injection strategy. Figure 10(c) shows a four-layer flow with a decreasing injection rate. With the addition of only one more fluid, the flow is less unstable than the three-layer flow with a constant injection rate. This demonstrates the using additional fluid layers, even a modest number, is a viable injection strategy even when the injection rate is chosen naively.

In this section, we numerically investigated two different time-dependent injection strategies. First, we considered the maximum injection rate for which the flow is stable. We found that for any number of fluid layers, the maximum stable injection rate is decreasing and proportional to $t^{-1/3}$ for $t \gg 1$. Additionally, the fluid can be injected faster while maintaining stability if the number of layers increases due to the sum of the interfacial tensions increasing. However, when considering a scenario in which the flow cannot be stabilized, for example when a certain amount of fluid must be injected in a given short amount of time, an increasing injection rate leads to a less unstable flow than a constant or decreasing injection rate. Regardless of the injection strategy, adding even one extra layer of fluid can significantly affect the stability.

V. CONCLUSION

In this paper, linear stability analysis is used to explore several different time-dependent injection strategies that can be used to control the instability of multilayer immiscible Hele-Shaw and porous

media flows. In applications like oil recovery, it can be advantageous to inject fluid as quickly as possible while maintaining a stable flow. For two-layer flows, the maximum injection rate for which a disturbance with a particular wave number is stable is given in Ref. [50]. A similar condition is found in the present work for three-layer flows by using Gershgorin's circle theorem. By using upper bounds derived in Ref. [56], a sufficient condition on the injection rate to ensure stability is found for a flow with an arbitrary number of fluid layers.

The maximum injection rate for a stable flow is then explored numerically. It is found that flows with more fluid layers can be stable with faster injection rates than comparable flows with fewer fluid layers, even when the intermediate fluid layers are very thin. It is shown that for flows with an arbitrary number of fluid layers the maximum stable injection rate is proportional to $t^{-1/3}$ for $t \gg 1$ with the constant of proportionality being proportional to the number of interfaces raised to the two-thirds power. We also show that when a certain amount of fluid must be injected in a fixed amount of time, an increasing injection rate can produce a less unstable flow than a comparable constant or decreasing injection strategy. Finally, we demonstrate that the addition of even a modest number of additional fluids can overcome even a poor injection strategy.

There are several important future directions of study. This paper contains theoretical results based on linear theory. Since the linear theory may fail after some time or at some length scale, it is necessary to perform physical experiments as well as full numerical simulations to explore the nonlinear effects. As evidenced by Ref. [58], which is a numerical study of three-layer flow with constant injection, these studies are likely to be very interesting, and may be even more so when the injection rate is time-dependent or the number layers is increased. The findings can be nontrivial and can provide insights into the physics of such multi-interfacial flows. There is also room within the linear theory to further explore the interfacial morphology and interactions between the interfaces, especially when the number of interfaces is large. Finally, it would be interesting to analyze the stability of multilayer radial flows with time-dependent injection in nonstandard geometries, such as in tapered Hele-Shaw cells or when the gap width is time dependent. The effects of different geometries would significantly alter the spectral problem which governs the growth of disturbances.

ACKNOWLEDGMENTS

This work has been supported in part by the US National Science Foundation Grant No. DMS-1522782. We sincerely thank the reviewers for useful suggestions which have helped us to improve the paper significantly.

APPENDIX: DERIVATIONS

In this Appendix, we give full derivations of the equations in Sec. II. The equations of motion are given by Eqs. (1), which can be written as

$$\frac{\partial u_r}{\partial r} + \frac{u_r}{r} + \frac{1}{r}\frac{\partial u_\theta}{\partial \theta} = 0, \quad \frac{\partial p}{\partial r} = -\frac{\mu}{\kappa}u_r, \quad \frac{1}{r}\frac{\partial p}{\partial \theta} = -\frac{\mu}{\kappa}u_\theta, \quad \text{for } r \neq 0. \tag{A1}$$

Recall the scaling given by Eqs. (2)–(9):

$$Q_{\text{ref}} = \frac{12\pi\kappa T_N}{R_N(0)\mu_o}, \quad Q^* = \frac{Q}{Q_{\text{ref}}}, \quad r^* = \frac{r}{R_N(0)}, \quad \mu^* = \frac{\mu}{\mu_o},$$

$$t^* = \frac{12\kappa T_N}{R_N^3(0)\mu_o}t, \quad \mathbf{u}^* = \frac{R_N^2(0)\mu_o}{12\kappa T_N}\mathbf{u}, \quad p^* = \frac{R_N(0)}{12T_N}p, \quad T^* = \frac{T}{T_N}.$$

From these scalings, the following substitutions can be derived:

$$Q = Q_{\text{ref}}Q^* = \frac{12\pi\kappa T_N Q^*}{R_N(0)\mu_o}, \tag{A2}$$

$$r = R_N(0)r^*, \tag{A3}$$

$$\frac{\partial}{\partial r} = \frac{\partial}{R_N(0)\partial r^*}, \tag{A4}$$

$$\mu = \mu_o \mu^*, \tag{A5}$$

$$\frac{\partial}{\partial t} = \frac{12\kappa T_N}{R_N^3(0)\mu_o}\frac{\partial}{\partial t^*}, \tag{A6}$$

$$\mathbf{u} = \frac{12\kappa T_N}{R_N^2(0)\mu_o}\mathbf{u}^*, \tag{A7}$$

$$p = \frac{12T_N}{R_N(0)}p^*, \tag{A8}$$

$$T_j = T_N T_j^*. \tag{A9}$$

Using (A3), (A4), and (A7) in Eq. $(A1)_1$,

$$\frac{12\kappa T_N}{R_N^2(0)\mu_o}\frac{\partial u_r^*}{R_N(0)\partial r^*} + \frac{12\kappa T_N}{R_N^2(0)\mu_o}\frac{u_r^*}{R_N(0)r^*} + \frac{1}{R_N(0)r^*}\frac{12\kappa T_N}{R_N^2(0)\mu_o}\frac{\partial u_\theta^*}{\partial\theta} = 0.$$

Dividing by the constant $(12\kappa T_N)/(R_N^3(0)\mu_o)$ yields

$$\nabla^* \cdot \mathbf{u}^* := \frac{\partial u_r^*}{\partial r^*} + \frac{u_r^*}{r^*} + \frac{1}{r^*}\frac{\partial u_\theta^*}{\partial\theta} = 0. \tag{A10}$$

Plugging (A4), (A5), (A7), and (A8) into Eq. $(A1)_2$,

$$\frac{12T_N}{R_N(0)}\frac{\partial p^*}{R_N(0)\partial r^*} = -\frac{\mu_o\mu^*}{\kappa}\frac{12\kappa T_N}{R_N^2(0)\mu_o}u_r^*.$$

Dividing by the constant $12T_N/R_N^2(0)$ gives

$$\frac{\partial p^*}{\partial r^*} = -\mu^* u_r^*. \tag{A11}$$

Plugging (A3), (A5), (A7), and (A8) into Eq. $(A1)_3$,

$$\frac{1}{R_N(0)r^*}\frac{12T_N}{R_N(0)}\frac{\partial p^*}{\partial\theta} = -\frac{\mu_o\mu^*}{\kappa}\frac{12\kappa T_N}{R_N^2(0)\mu_o}u_\theta^*.$$

Dividing by the constant $12T_N/R_N^2(0)$ yields

$$\frac{1}{r^*}\frac{\partial p^*}{\partial\theta} = -\mu^* u_\theta^*. \tag{A12}$$

Equations (A10)–(A12) can be collectively written as

$$\nabla^* \cdot \mathbf{u}^* = 0, \quad \nabla^* p^* = -\mu^* \mathbf{u}^*, \quad \text{for } r^* \neq 0, \tag{A13}$$

The original equations admit a simple basic solution in which all of the fluid moves outward radially with velocity $\mathbf{u} := (u_r, u_\theta) = (Q/(2\pi r), 0)$. The interfaces remain circular and move outward with velocity $dR_j/dt = Q/(2\pi R_j(t))$ for $j = 0, ..., N$. Using Eqs. (A2), (A3), and (A7), the basic solution $\mathbf{u}^*$ in the scaled variables satisfies

$$\frac{12\kappa T_N}{R_N^2(0)\mu_o}\mathbf{u}^* = \frac{12\pi\kappa T_N Q^*}{2\pi R_N^2(0)\mu_o r^*}.$$

Dividing by the constant $12\kappa T_N/(R_N^2(0)\mu_o)$ gives

$$\mathbf{u}^* = \frac{Q^*}{2r^*}. \tag{A14}$$

Equation (A3) implies that $R_j(t) = R_N(0)R_j^*(t^*)$ for all j. Using this along with Eqs. (A2) and (A6), the circular interfaces of the basic solution move outward radially with velocity dR_j^*/dt^* which satisfy

$$\frac{12\kappa T_N}{R_N^2(0)\mu_o}\frac{dR_j^*}{dt^*} = \frac{12\pi\kappa T_N Q^*}{2\pi R_N^2(0)\mu_o R_j^*}.$$

Dividing by $12\kappa T_N/(R_N^2(0)\mu_o)$ gives

$$\frac{dR_j^*}{dt^*} = \frac{Q^*}{2R_j^*}. \tag{A15}$$

For notational convenience, we drop the stars below.

We perturb the basic solution (u_r, u_θ, p) by $(\tilde{u}_r, \tilde{u}_\theta, \tilde{p})$ where the disturbances are assumed to be small. We plug these into Eqs. (A13) and only keep terms that are linear with respect to disturbances. Since Eqs. (A13) are, in fact, linear, the disturbances satisfy the same equations. Therefore,

$$\frac{\partial\tilde{u}_r}{\partial r} + \frac{\tilde{u}_r}{r} + \frac{1}{r}\frac{\partial\tilde{u}_\theta}{\partial\theta} = 0, \quad \frac{\partial\tilde{p}}{\partial r} = -\mu\tilde{u}_r, \quad \frac{1}{r}\frac{\partial\tilde{p}}{\partial\theta} = -\mu\tilde{u}_\theta. \tag{A16}$$

We use separation of variables and assume that the disturbances are of the form

$$(\tilde{u}_r, \tilde{u}_\theta, \tilde{p}) = (f(r), \tau(r), \psi(r))g(t)e^{in\theta}. \tag{A17}$$

Using Eq. (A17) in Eq. $(A16)_1$,

$$f'(r)g(t)e^{in\theta} + \frac{1}{r}f(r)g(t)e^{in\theta} + \frac{in}{r}\tau(r)g(t)e^{in\theta} = 0.$$

Simplifying,

$$f'(r) + \frac{1}{r}f(r) + \frac{in}{r}\tau(r) = 0$$

and therefore,

$$\tau(r) = \frac{i}{n}(f(r) + rf'(r)). \tag{A18}$$

Next, we use Eq. (A17) in Eq. $(A16)_3$ which yields,

$$\frac{in}{r}\psi(r)g(t)e^{in\theta} = -\mu\tau(r)g(t)e^{in\theta}.$$

Simplifying,

$$\psi(r) = \frac{ir\mu}{n}\tau(r). \tag{A19}$$

Using Eq. (A18) in Eq. (A19),

$$\psi(r) = -\frac{r\mu}{n^2}(f(r) + rf'(r)). \tag{A20}$$

We now cross-differentiate the pressure Eqs. $(A16)_2$ and $(A16)_3$. Taking $\frac{\partial}{\partial\theta}$ of Eq. $(A16)_2$ and $\frac{\partial}{\partial r}$ of Eq. $(A16)_3$ yields

$$\frac{\partial^2\tilde{p}}{\partial r\partial\theta} = -\mu\frac{\partial\tilde{u}_r}{\partial\theta}, \quad \frac{\partial^2\tilde{p}}{\partial\theta\partial r} = \frac{1}{r}\frac{\partial\tilde{p}}{\partial\theta} - r\mu\frac{\partial\tilde{u}_\theta}{\partial r}.$$

Setting these equal gives

$$-\mu\frac{\partial\tilde{u}_r}{\partial\theta} = \frac{1}{r}\frac{\partial\tilde{p}}{\partial\theta} - r\mu\frac{\partial\tilde{u}_\theta}{\partial r}. \tag{A21}$$

We use the ansatz Eq. (A17) in Eq. (A21) and get

$$-i\,\mu\, n f(r) g(t) e^{in\theta} = \frac{in}{r}\psi(r) g(t) e^{in\theta} - r\mu\tau'(r) g(t) e^{in\theta}.$$

Using Eqs. (A18) and (A19),

$$-i\,\mu\, n f(r) = -\mu\frac{i}{n}(f(r) + r f'(r)) - r\mu\frac{i}{n}(2f'(r) + r f''(r)).$$

With some algebraic manipulation, we get the following ordinary differential equation for $f(r)$:

$$(r^3 f'(r))' - (n^2 - 1) r f(r) = 0. \tag{A22}$$

The above equation is exact since there has been no linearization in its derivation.

Next we derive the boundary conditions for this equation from linearization of the kinematic and dynamic interfacial boundary conditions. Let the disturbance of the interface located at $R_j(t)$ be given by $a_n^j(t,\theta) = A_n^j(t) e^{in\theta}$. The linearized kinematic interface conditions (see Appendix A 1) are given by

$$\frac{\partial a_n^j}{\partial t} = \tilde{u}_r(R_j) - a_n^j \frac{Q}{2R_j^2}, \tag{A23}$$

where $\tilde{u}_r$ is continuous at $r = R_j$. Here, the interface condition has been taken at the linearized position $r = R_j$. Using $a_n^j = A_n^j(t) e^{in\theta}$ and the ansatz Eq. (A17) in Eq. (A23),

$$\frac{dA_n^j(t)}{dt} = f(R_j) g(t) - A_n^j(t) \frac{Q}{2R_j^2}. \tag{A24}$$

The linearized dynamic interface condition (see Appendix A 1) at the innermost interface located at $R = R_0$ is

$$\left\{\tilde{p}^+(R_0) - a_n^0 \frac{Q\mu_1}{2R_0}\right\} - \left\{\tilde{p}^-(R_0) - a_n^0 \frac{Q\mu_i}{2R_0}\right\} = \frac{T_0}{12}\frac{a_n^0 + \frac{\partial^2 a_n^0}{\partial\theta^2}}{R_0^2},$$

where T_0 is the interfacial tension of the inner interface and the superscripts + and – denote the limits from above and below, respectively. Using $a_n^0 = A_n^0(t) e^{in\theta}$ and the ansatz Eq. (A17),

$$\left\{\psi^+(R_0) g(t) e^{in\theta} - A_n^0(t) e^{in\theta}\frac{Q\mu_1}{2R_0}\right\} - \left\{\psi^-(R_0) g(t) e^{in\theta} - A_n^0(t) e^{in\theta}\frac{Q\mu_i}{2R_0}\right\} = \frac{T_0}{12}\frac{1-n^2}{R_0^2} A_n^0(t) e^{in\theta}.$$

Using Eq. (A20),

$$\begin{aligned} &-\frac{R_0\mu_1}{n^2}(f(R_0) + R_0(f^+)'(R_0)) g(t) - A_n^0(t)\frac{Q\mu_1}{2R_0} \\ &+\frac{R_0\mu_i}{n^2}(f(R_0) + R_0(f^-)'(R_0)) g(t) + A_n^0(t)\frac{Q\mu_i}{2R_0} = \frac{T_0}{12}\frac{1-n^2}{R_0^2} A_n^0(t). \end{aligned}$$

After some algebraic manipulation,

$$\begin{aligned} &\{f(R_0)(\mu_i - \mu_1) + R_0[\mu_i (f^-)'(R_0) - \mu_1 (f^+)'(R_0)]\} g(t) \\ &\quad = \left\{\frac{Qn^2}{2R_0^2}(\mu_1 - \mu_i) - \frac{T_0}{12}\frac{n^4 - n^2}{R_0^3}\right\} A_n^0(t). \end{aligned} \tag{A25}$$

The linearized dynamic condition at the outermost interface located at $R = R_N$ is

$$\left\{\tilde{p}^+(R_N) - a_n^N \frac{Q}{2R_N}\right\} - \left\{\tilde{p}^-(R_N) - a_n^N \frac{Q\mu_N}{2R_N}\right\} = \frac{1}{12}\frac{a_n^N + \frac{\partial^2 a_n^N}{\partial\theta^2}}{R_N^2},$$

where T_N is the interfacial tension of the outermost interface. Using $a_n^N = A_n^N(t)e^{in\theta}$ and the ansatz Eq. (A17),

$$\left\{\psi^+(R_N)g(t)e^{in\theta} - A_n^N(t)e^{in\theta}\frac{Q}{2R_N}\right\} - \left\{\psi^-(R_N)g(t)e^{in\theta} - A_n^N(t)e^{in\theta}\frac{Q\mu_N}{2R_N}\right\}$$
$$= \frac{1}{12}\frac{1-n^2}{R_N^2}A_n^N(t)e^{in\theta}.$$

Using Eq. (A20),

$$-\frac{R_N}{n^2}(f(R_N) + R_N(f^+)'(R_N))g(t) - A_n^N(t)\frac{Q}{2R_N}$$
$$+\frac{R_N\mu_N}{n^2}(f(R_N) + R_N(f^-)'(R_N))g(t) + A_n^N(t)\frac{Q\mu_N}{2R_N} = \frac{1}{12}\frac{1-n^2}{R_N^2}A_n^N(t).$$

After some algebraic manipulation,

$$\{f(R_N)(\mu_N - 1) + R_N[\mu_N(f^-)'(R_N) - (f^+)'(R_N)]\}g(t)$$
$$= \left\{\frac{Qn^2}{2R_N^2}(1-\mu_N) - \frac{1}{12}\frac{n^4-n^2}{R_N^3}\right\}A_n^N(t). \tag{A26}$$

For any intermediate interface at $R = R_j$, the dynamic interface condition is

$$\left\{\tilde{p}^+(R_j) - a_n^j\frac{Q\mu_{j+1}}{2R_j}\right\} - \left\{\tilde{p}^-(R_j) - a_n^j\frac{Q\mu_j}{2R_j}\right\} = \frac{T_j}{12}\frac{a_n^j + \frac{\partial^2 a_n^j}{\partial\theta^2}}{R_j^2},$$

where T_j is the interfacial tension of the interface at $R = R_j$. Using $a_n^j = A_n^j(t)e^{in\theta}$ and the ansatz Eq. (A17),

$$\left\{\psi^+(R_j)g(t)e^{in\theta} - A_n^j(t)e^{in\theta}\frac{Q\mu_{j+1}}{2R_j}\right\} - \left\{\psi^-(R_j)g(t)e^{in\theta} - A_n^j(t)e^{in\theta}\frac{Q\mu_j}{2R_j}\right\} = \frac{T_j}{12}\frac{1-n^2}{R_j^2}A_n^j(t)e^{in\theta}.$$

Using Eq. (A20),

$$-\frac{R_j\mu_{j+1}}{n^2}(f(R_j) + R_j(f^+)'(R_j))g(t) - A_n^j(t)\frac{Q\mu_{j+1}}{2R_j}$$
$$+\frac{R_j\mu_j}{n^2}(f(R_j) + R_j(f^-)'(R_j))g(t) + A_n^j(t)\frac{Q\mu_j}{2R_j} = \frac{T_j}{12}\frac{1-n^2}{R_j^2}A_n^j(t).$$

After some algebraic manipulation,

$$\{f(R_j)(\mu_j - \mu_{j+1}) + R_j[\mu_j(f^-)'(R_j) - \mu_{j+1}(f^+)'(R_j)]\}g(t)$$
$$= \left\{\frac{Qn^2}{2R_j^2}(\mu_{j+1} - \mu_j) - \frac{T_j}{12}\frac{n^4-n^2}{R_j^3}\right\}A_n^j(t). \tag{A27}$$

Recall that $f(r)$ satisfies Eq. (A22). Solutions of Eq. (A22) are of the form

$$f(r) = \begin{cases} K_{i,1}r^{n-1} + K_{i,2}r^{-(n+1)}, & r < R_0 \\ K_{j,1}r^{n-1} + K_{j,2}r^{-(n+1)}, & R_{j-1} < r < R_j, \quad j = 1, ..., N \\ K_{o,1}r^{n-1} + K_{o,2}r^{-(n+1)}, & r > R_N. \end{cases}$$

To ensure that the disturbances go to zero as $r \to \infty$ and to avoid a singularity at $r = 0$, we require that $K_{i,2} = 0$ and $K_{o,1} = 0$. Therefore,

$$(f^-)'(R_0) = \frac{(n-1)f(R_0)}{R_0}, \quad (f^+)'(R_N) = -\frac{(n+1)f(R_N)}{R_N}. \tag{A28}$$

The solution to Eq. (A22) for $R_{j-1} < r < R_j$ can also be written as

$$f(r) = \frac{\left[f(R_j)\left(\frac{R_{j-1}}{R_j}\right)^{n-1} - f(R_{j-1})\right]\left(\frac{r}{R_{j-1}}\right)^{-n-1} + \left[f(R_{j-1})\left(\frac{R_{j-1}}{R_j}\right)^{n+1} - f(R_j)\right]\left(\frac{r}{R_j}\right)^{n-1}}{\left(\frac{R_{j-1}}{R_j}\right)^{2n} - 1}, \tag{A29}$$

for $j = 1, ..., N$. Taking a derivative of this function and evaluating at R_{j-1} and R_j,

$$\begin{aligned}(f^+)'(R_{j-1}) &= \frac{n}{R_{j-1}} \frac{f(R_{j-1})\left[\left(\frac{R_{j-1}}{R_j}\right)^{2n} + 1\right] - 2f(R_j)\left(\frac{R_{j-1}}{R_j}\right)^{n-1}}{\left(\frac{R_{j-1}}{R_j}\right)^{2n} - 1} - \frac{f(R_{j-1})}{R_{j-1}}, \\ (f^-)'(R_j) &= -\frac{n}{R_j} \frac{f(R_j)\left[\left(\frac{R_{j-1}}{R_j}\right)^{2n} + 1\right] - 2f(R_{j-1})\left(\frac{R_{j-1}}{R_j}\right)^{n+1}}{\left(\frac{R_{j-1}}{R_j}\right)^{2n} - 1} - \frac{f(R_j)}{R_j}.\end{aligned} \tag{A30}$$

Using Eqs. $(A28)_1$ and $(A30)_1$ with $j = 1$ in the interface condition Eq. (A25),

$$\begin{aligned}&\left\{f(R_0)(\mu_i - \mu_1) + \mu_i(n-1)f(R_0) - \mu_1 n \frac{f(R_0)\left[\left(\frac{R_0}{R_1}\right)^{2n} + 1\right] - 2f(R_1)\left(\frac{R_0}{R_1}\right)^{n-1}}{\left(\frac{R_0}{R_1}\right)^{2n} - 1} + \mu_1 f(R_0)\right\} g(t) \\ &= \left\{\frac{Qn^2}{2R_0^2}(\mu_1 - \mu_i) - \frac{T_0}{12}\frac{n^4 - n^2}{R_0^3}\right\} A_n^0(t).\end{aligned}$$

Simplifying,

$$\begin{aligned}&\left\{n\mu_i f(R_0) - \mu_1 n \frac{f(R_0)\left[\left(\frac{R_0}{R_1}\right)^{2n} + 1\right] - 2f(R_1)\left(\frac{R_0}{R_1}\right)^{n-1}}{\left(\frac{R_0}{R_1}\right)^{2n} - 1}\right\} g(t) \\ &= \left\{\frac{Qn^2}{2R_0^2}(\mu_1 - \mu_i) - \frac{T_0}{12}\frac{n^4 - n^2}{R_0^3}\right\} A_n^0(t).\end{aligned}$$

After further algebraic manipulation,

$$\left\{\mu_i - \mu_1 \frac{\left(\frac{R_0}{R_1}\right)^{2n} + 1}{\left(\frac{R_0}{R_1}\right)^{2n} - 1}\right\} f(R_0)g(t) + 2\mu_1 \frac{\left(\frac{R_0}{R_1}\right)^{n-1}}{\left(\frac{R_0}{R_1}\right)^{2n} - 1} f(R_1)g(t) = F_0 A_n^0(t), \tag{A31}$$

where

$$F_0 = \frac{Qn}{2R_0^2}(\mu_1 - \mu_i) - \frac{T_0}{12}\frac{n^3 - n}{R_0^3}. \tag{A32}$$

Using Eqs. $(A28)_2$ and $(A30)_2$ with $j = N$ in the interface condition Eq. (A26),

$$\begin{aligned}&\left\{f(R_N)(\mu_N - 1) - \mu_N n \frac{f(R_N)\left[\left(\frac{R_{N-1}}{R_N}\right)^{2n} + 1\right] - 2f(R_{N-1})\left(\frac{R_{N-1}}{R_N}\right)^{n+1}}{\left(\frac{R_{N-1}}{R_N}\right)^{2n} - 1}\right. \\ &\left. - \mu_N f(R_N) + (n+1)f(R_N)\right\} g(t) = \left\{\frac{Qn^2}{2R_N^2}(1 - \mu_N) - \frac{1}{12}\frac{n^4 - n^2}{R_N^3}\right\} A_n^N(t).\end{aligned}$$

Simplifying,

$$\left\{-\mu_N n\frac{f(R_N)\left[\left(\frac{R_{N-1}}{R_N}\right)^{2n}+1\right]-2f(R_{N-1})\left(\frac{R_{N-1}}{R_N}\right)^{n+1}}{\left(\frac{R_{N-1}}{R_N}\right)^{2n}-1}+nf(R_N)\right\}g(t)$$
$$=\left\{\frac{Qn^2}{2R_N^2}(1-\mu_N)-\frac{1}{12}\frac{n^4-n^2}{R_N^3}\right\}A_n^N(t).$$

After further algebraic manipulation,

$$\left\{1-\mu_N\frac{\left(\frac{R_{N-1}}{R_N}\right)^{2n}+1}{\left(\frac{R_{N-1}}{R_N}\right)^{2n}-1}\right\}f(R_N)g(t)+2\mu_N\frac{\left(\frac{R_{N-1}}{R_N}\right)^{n+1}}{\left(\frac{R_{N-1}}{R_N}\right)^{2n}-1}f(R_{N-1})g(t)=F_NA_n^N(t), \tag{A33}$$

where

$$F_N=\frac{Qn}{2R_N^2}(1-\mu_N)-\frac{1}{12}\frac{n^3-n}{R_N^3}. \tag{A34}$$

For the intermediate interfaces, we use Eq. (A30) in the interface condition Eq. (A27),

$$\left\{f(R_j)(\mu_j-\mu_{j+1})-n\mu_j\frac{f(R_j)\left[\left(\frac{R_{j-1}}{R_j}\right)^{2n}+1\right]-2f(R_{j-1})\left(\frac{R_{j-1}}{R_j}\right)^{n+1}}{\left(\frac{R_{j-1}}{R_j}\right)^{2n}-1}-\mu_jf(R_j)\right.$$
$$\left.-n\mu_{j+1}\frac{f(R_j)\left[\left(\frac{R_j}{R_{j+1}}\right)^{2n}+1\right]-2f(R_{j+1})\left(\frac{R_j}{R_{j+1}}\right)^{n-1}}{\left(\frac{R_j}{R_{j+1}}\right)^{2n}-1}+\mu_{j+1}f(R_j)\right\}g(t)$$
$$=\left\{\frac{Qn^2}{2R_j^2}(\mu_{j+1}-\mu_j)-\frac{T_j}{12}\frac{n^4-n^2}{R_j^3}\right\}A_n^j(t).$$

Simplifying,

$$\left\{-n\mu_j\frac{f(R_j)\left[\left(\frac{R_{j-1}}{R_j}\right)^{2n}+1\right]-2f(R_{j-1})\left(\frac{R_{j-1}}{R_j}\right)^{n+1}}{\left(\frac{R_{j-1}}{R_j}\right)^{2n}-1}\right.$$
$$\left.-n\mu_{j+1}\frac{f(R_j)\left[\left(\frac{R_j}{R_{j+1}}\right)^{2n}+1\right]-2f(R_{j+1})\left(\frac{R_j}{R_{j+1}}\right)^{n-1}}{\left(\frac{R_j}{R_{j+1}}\right)^{2n}-1}\right\}g(t)$$
$$=\left\{\frac{Qn^2}{2R_j^2}(\mu_{j+1}-\mu_j)-\frac{T_j}{12}\frac{n^4-n^2}{R_j^3}\right\}A_n^j(t).$$

After further algebraic manipulation,

$$\left\{-\mu_j\frac{\left(\frac{R_{j-1}}{R_j}\right)^{2n}+1}{\left(\frac{R_{j-1}}{R_j}\right)^{2n}-1}-\mu_{j+1}\frac{\left(\frac{R_j}{R_{j+1}}\right)^{2n}+1}{\left(\frac{R_j}{R_{j+1}}\right)^{2n}-1}\right\}f(R_j)g(t)$$
$$+2\mu_j\frac{\left(\frac{R_{j-1}}{R_j}\right)^{n+1}}{\left(\frac{R_{j-1}}{R_j}\right)^{2n}-1}f(R_{j-1})g(t)+2\mu_{j+1}\frac{\left(\frac{R_j}{R_{j+1}}\right)^{n-1}}{\left(\frac{R_j}{R_{j+1}}\right)^{2n}-1}f(R_{j+1})g(t)=F_jA_n^j(t), \tag{A35}$$

where

$$F_j = \frac{Qn}{2R_j^2}(\mu_{j+1} - \mu_j) - \frac{T_j}{12}\frac{n^3 - n}{R_j^3}, \quad j = 1, \ldots, N-1. \tag{A36}$$

Linearized interface conditions

First, we derive the linearized interface conditions in the original dimensional variables. Then we will apply the scaling given by Eqs. (2)–(9) to obtain them in dimensionless form.

Let the disturbance of the interface located at $R_j(t)$ be given by $a_n^j(t,\theta)$. Therefore, the radial position of the interface is $\eta(t,\theta) = R_j(t) + a_n^j(t,\theta)$. The kinematic condition is given by

$$\frac{D\eta}{Dt} = \mathbf{u}\cdot\hat{\mathbf{n}}, \quad r = \eta(t,\theta), \tag{A37}$$

where D/Dt denotes the material derivative, $\mathbf{u} := (u_r, u_\theta)$ is the velocity in polar coordinates, and $\hat{\mathbf{n}}$ denotes the unit vector which is normal to the interface. Using that $\eta(t,\theta) = R_j(t) + a_n^j(t,\theta)$, the left-hand side of this equation can be rewritten as

$$\frac{D\eta}{Dt} = \frac{dR_j(t)}{dt} + \frac{Da_n^j}{Dt} = \frac{Q}{2\pi R_j} + \frac{\partial a_n^j}{\partial t} + \frac{u_\theta}{r}\frac{\partial a_n^j}{\partial \theta}. \tag{A38}$$

The unit normal vector is given by

$$\hat{\mathbf{n}} = \frac{\left(1, -\frac{1}{r}\frac{\partial\eta}{\partial\theta}\right)}{\sqrt{1 + \left(\frac{1}{r}\frac{\partial\eta}{\partial\theta}\right)^2}}. \tag{A39}$$

Using Eqs. (A38) and (A39), the kinematic condition Eq. (A37) is

$$\frac{Q}{2\pi R_j} + \frac{\partial a_n^j}{\partial t} + \frac{u_\theta}{r}\frac{\partial a_n^j}{\partial\theta} = \frac{u_r - \frac{u_\theta}{r}\frac{\partial\eta}{\partial\theta}}{\sqrt{1 + \left(\frac{1}{r}\frac{\partial\eta}{\partial\theta}\right)^2}}, \quad r = \eta(t,\theta), \tag{A40}$$

We expand each term that depends on r in a Taylor series about $r = R_j$. To do so, we first recall that the velocity of the basic solution is $(Q/(2\pi r), 0)$ and the disturbance of the velocity is $(\tilde{u}_r, \tilde{u}_\theta)$. Therefore, the components of velocity are

$$u_r = \frac{Q}{2\pi r} + \tilde{u}_r, \quad u_\theta = \tilde{u}_\theta. \tag{A41}$$

Using this expression for u_r and that $\eta(t,\theta) = R_j(t) + a_n^j(t,\theta)$, we get the following expression for $u_r(\eta)$:

$$u_r(\eta) = u_r(R_j) + a_n^j\frac{\partial u_r}{\partial r}(R_j) + \mathcal{O}\left(\left|a_n^j\right|^2\right) = \frac{Q}{2\pi R_j} + \tilde{u}_r(R_j) + a_n^j\frac{\partial}{\partial r}\left(\frac{Q}{2\pi r}\right)\Big|_{r=R_j}$$
$$+ a_n^j\frac{\partial\tilde{u}_r}{\partial r}(R_j) + \mathcal{O}\left(\left|a_n^j\right|^2\right).$$

Keeping only terms that are linear with respect to disturbances,

$$u_r(\eta) = \frac{Q}{2\pi R_j} + \tilde{u}_r(R_j) - a_n^j \frac{Q}{2\pi R_j^2}. \tag{A42}$$

Likewise, the Taylor series expansion for $u_\theta(\eta)$ about $r = R_j$ is

$$u_\theta(\eta) = u_\theta(R_j) + a_n^j \frac{\partial u_\theta}{\partial r}(R_j) + \mathcal{O}\left(\left|a_n^j\right|^2\right) = \tilde{u}_\theta(R_j) + a_n^j \frac{\partial \tilde{u}_\theta}{\partial r}(R_j) + \mathcal{O}\left(\left|a_n^j\right|^2\right).$$

Keeping only linear terms,

$$u_\theta(\eta) = \tilde{u}_\theta(R_j). \tag{A43}$$

Plugging Eqs. (A42) and (A43) into Eq. (A40),

$$\frac{Q}{2\pi R_j} + \frac{\partial a_n^j}{\partial t} + \frac{\tilde{u}_\theta(R_j)}{r}\frac{\partial a_n^j}{\partial \theta} = \frac{\frac{Q}{2\pi R_j} + \tilde{u}_r(R_j) - a_n^j \frac{Q}{2\pi R_j^2} - \frac{\tilde{u}_\theta(R_j)}{r}\frac{\partial a_n^j}{\partial \theta}}{\sqrt{1 + \left(\frac{1}{r}\frac{\partial a_n^j}{\partial \theta}\right)^2}}, \quad r = \eta(t,\theta),$$

where we used that $\partial\eta/\partial\theta = \partial a_n^j/\partial\theta$. Linearizing with respect to the disturbances and canceling like terms leads to the linearized kinematic interface condition:

$$\frac{\partial a_n^j}{\partial t} = \tilde{u}_r(R_j) - a_n^j \frac{Q}{2\pi R_j^2}. \tag{A44}$$

Next, we derive the linearized dynamic interface condition. The dynamic interface condition is

$$[p] = -T_j \nabla \cdot \hat{\mathbf{n}}, \quad r = \eta(t,\theta), \tag{A45}$$

where $[p]$ denotes the jump in pressure across the interface and T_j denotes the interfacial tension. Let p_b denote the pressure of the basic solution and $\tilde{p}$ denote the disturbance of the pressure so that $p = p_b + \tilde{p}$. Using a Taylor series expansion about $r = R_j$, the pressure is given by

$$\begin{aligned} p(\eta) &= p(R_j) + a_n^j \frac{\partial p}{\partial r}(R_j) + \mathcal{O}\left(\left|a_n^j\right|^2\right) \\ &= p_b(R_j) + \tilde{p}(R_j) + a_n^j \frac{\partial p_b}{\partial r}(R_j) + a_n^j \frac{\partial \tilde{p}}{\partial r}(R_j) + \mathcal{O}\left(\left|a_n^j\right|^2\right). \end{aligned}$$

We wish to evaluate the term $[p] := \lim_{r\to\eta^+} p(r) - \lim_{r\to\eta^-} p(r)$. We denote the pressure in the fluid region immediately inside the interface as p^- and the pressure in the fluid region immediately outside the interface as p^+. Then, using the Taylor series expansion above,

$$\begin{aligned} [p] = &\lim_{r\to R_j^+} \left\{ p_b^+(r) + \tilde{p}^+(r) + a_n^j \frac{\partial p_b^+}{\partial r}(r) + a_n^j \frac{\partial \tilde{p}^+}{\partial r}(r) + O\left(\left|a_n^j\right|^2\right) \right\} \\ &- \lim_{r\to R_j^-} \left\{ p_b^-(r) + \tilde{p}^-(r) + a_n^j \frac{\partial p_b^-}{\partial r}(r) + a_n^j \frac{\partial \tilde{p}^-}{\partial r}(r) + O\left(\left|a_n^j\right|^2\right) \right\}. \end{aligned}$$

We then linearize this equation and use from Eq. $(A1)_2$ that $\partial p_b/\partial r = -(Q\mu)/(2\pi\kappa r)$ to get

$$[p] = \lim_{r\to R_j^+} \left\{ p_b^+(r) + \tilde{p}^+(r) - a_n^j \frac{Q\mu(r)}{2\pi\kappa r} \right\} - \lim_{r\to R_j^-} \left\{ p_b^-(r) + \tilde{p}^-(r) - a_n^j \frac{Q\mu(r)}{2\pi\kappa r} \right\}. \tag{A46}$$

Note that for the basic solution, the interface is circular with radius $r = R_j$, and therefore $\nabla \cdot \hat{\mathbf{n}} = 1/R_j$. Plugging this into the dynamic interface condition Eq. (A45),

$$[p_b] = -\frac{T_j}{R_j}.$$

Using this in Eq. (A46),

$$[p] = \lim_{r\to R_j^+}\left\{\tilde{p}^+(r) - a_n^j\frac{Q\mu(r)}{2\pi\kappa r}\right\} - \lim_{r\to R_j^-}\left\{\tilde{p}^-(r) - a_n^j\frac{Q\mu(r)}{2\pi\kappa r}\right\} - \frac{T_j}{R_j}. \tag{A47}$$

Using Eq. (A39) for the unit normal vector, the curvature of the interface is

$$\begin{aligned}\nabla\cdot\hat{\mathbf{n}} &= \frac{1}{r}\frac{\partial}{\partial r}\left(\frac{r}{\sqrt{1+\left(\frac{1}{r}\frac{\partial\eta}{\partial\theta}\right)^2}}\right) + \frac{1}{r}\frac{\partial}{\partial\theta}\left(-\frac{\frac{1}{r}\frac{\partial\eta}{\partial\theta}}{\sqrt{1+\left(\frac{1}{r}\frac{\partial\eta}{\partial\theta}\right)^2}}\right)\\ &= \frac{1}{r}\left\{\frac{1}{\sqrt{1+\left(\frac{1}{r}\frac{\partial a_n^j}{\partial\theta}\right)^2}} + \frac{\frac{1}{r^2}\left(\frac{\partial a_n^j}{\partial\theta}\right)^2}{\left(1+\left(\frac{1}{r}\frac{\partial a_n^j}{\partial\theta}\right)^2\right)^{\frac{3}{2}}} - \frac{\frac{1}{r}\frac{\partial^2 a_n^j}{\partial\theta^2}}{\sqrt{1+\left(\frac{1}{r}\frac{\partial a_n^j}{\partial\theta}\right)^2}} + \frac{\frac{1}{r^2}\left(\frac{\partial a_n^j}{\partial\theta}\right)^2\frac{\partial^2 a_n^j}{\partial\theta^2}}{\left(1+\left(\frac{1}{r}\frac{\partial a_n^j}{\partial\theta}\right)^2\right)^{\frac{3}{2}}}\right\},\end{aligned}$$

where we again used that $\partial\eta/\partial\theta = \partial a_n^j/\partial\theta$. Linearizing with respect to the disturbances,

$$\nabla\cdot\hat{\mathbf{n}} = \frac{1}{r} - \frac{1}{r^2}\frac{\partial^2 a_n^j}{\partial\theta^2}\bigg|_{r=R_j+a_n^j}.$$

We can expand this into a Taylor series about the point $r = R_j$ to get

$$\nabla\cdot\hat{\mathbf{n}} = \frac{1}{R_j} - \frac{a_n^j}{R_j^2} - \frac{1}{R_j^2}\frac{\partial^2 a_n^j}{\partial\theta^2} + O\left(\left|a_n^j\right|^2\right).$$

Again, we keep only terms which are linear with respect to the disturbances. Using this equation and Eq. (A47) in the interface condition Eq. (A45), we get

$$\lim_{r\to R_j^+}\left\{\tilde{p}^+(r) - a_n^j\frac{Q\mu(r)}{2\pi\kappa r}\right\} - \lim_{r\to R_j^-}\left\{\tilde{p}^-(r) - a_n^j\frac{Q\mu(r)}{2\pi\kappa r}\right\} - \frac{T_j}{R_j} = -T_j\left(\frac{1}{R_j} - \frac{a_n^j}{R_j^2} - \frac{1}{R_j^2}\frac{\partial^2 a_n^j}{\partial\theta^2}\right),$$

which simplifies to

$$\lim_{r\to R_j^+}\left\{\tilde{p}^+(r) - a_n^j\frac{Q\mu(r)}{2\pi\kappa r}\right\} - \lim_{r\to R_j^-}\left\{\tilde{p}^-(r) - a_n^j\frac{Q\mu(r)}{2\pi\kappa r}\right\} = T_j\frac{a_n^j + \frac{\partial^2 a_n^j}{\partial\theta^2}}{R_j^2}. \tag{A48}$$

Equations (A44) and (A48) are the linearized kinematic and dynamic interface conditions.

We now apply the scaling Eqs. (2)–(9) to obtain the linearized interface conditions in dimensionless form. Note that since a_n^j is a radial disturbance to the interface, Eq. (A3) implies that

$$a_n^j = R_N(0)\left(a_n^j\right)^*, \tag{A49}$$

where $(a_n^j)^*$ denotes the dimensionless disturbance. For the linearized kinematic condition, we use Eqs. (A2), (A3), (A6), (A7), and (A49) in Eq. (A44) to get

$$\frac{12R_N(0)\kappa T_N}{R_N^3(0)\mu_o}\frac{\partial\left(a_n^j\right)^*}{\partial t^*} = \frac{12\kappa T_N}{R_N^2(0)\mu_o}\tilde{u}_r^*(R_j^*) - R_N(0)\left(a_n^j\right)^*\left(\frac{12\pi\kappa T_N}{R_N(0)\mu_o}\right)\left(\frac{Q^*}{2\pi R_N^2(0)(R_j^*)^2}\right).$$

Dividing by the constant $12\kappa T_N/(R_N^2(0)\mu_o)$ gives

$$\frac{\partial\left(a_n^j\right)^*}{\partial t^*} = \tilde{u}_r^*(R_j^*) - \left(a_n^j\right)^*\frac{Q^*}{2(R_j^*)^2}. \tag{A50}$$

For the linearized dynamic interface condition, using Eqs. (A2), (A3), (A5), (A8), (A9), and (A49) in Eq. (A48) yields

$$\lim_{r^*\to(R_j^*)^+}\left\{\frac{12T_N}{R_N(0)}(\tilde{p}^*)^+(r)-R_N(0)\left(a_n^j\right)^*\left(\frac{12\pi\kappa T_N}{R_N(0)\mu_o}\right)\left(\frac{Q^*\mu_o\mu^*(r)}{2\pi\kappa R_N(0)r^*}\right)\right\}$$
$$-\lim_{r^*\to(R_j^*)^-}\left\{\frac{12T_N}{R_N(0)}(\tilde{p}^*)^-(r)-R_N(0)\left(a_n^j\right)^*\left(\frac{12\pi\kappa T_N}{R_N(0)\mu_o}\right)\left(\frac{Q^*\mu_o\mu^*(r)}{2\pi\kappa R_N(0)r^*}\right)\right\}$$
$$=T_NT_j^*\frac{R_N(0)\left(a_n^j\right)^*+R_N(0)\frac{\partial^2(a_n^j)^*}{\partial\theta^2}}{R_N^2(0)(R_j^*)^2}.$$

After some algebraic manipulation,

$$\lim_{r^*\to(R_j^*)^+}\left\{\frac{12T_N}{R_N(0)}(\tilde{p}^*)^+(r)-\frac{12T_N}{R_N(0)}\left(a_n^j\right)^*\frac{Q^*\mu^*(r)}{2r^*}\right\}$$
$$-\lim_{r^*\to(R_j^*)^-}\left\{\frac{12T_N}{R_N(0)}(\tilde{p}^*)^-(r)-\frac{12T_N}{R_N(0)}\left(a_n^j\right)^*\frac{Q^*\mu^*(r)}{2r^*}\right\}=\frac{T_N}{R_N(0)}T_j^*\frac{\left(a_n^j\right)^*+\frac{\partial^2(a_n^j)^*}{\partial\theta^2}}{(R_j^*)^2}.$$

Dividing by $12T_N/R_N(0)$,

$$\lim_{r^*\to(R_j^*)^+}\left\{(\tilde{p}^*)^+(r)-\left(a_n^j\right)^*\frac{Q^*\mu^*(r)}{2r^*}\right\}-\lim_{r^*\to(R_j^*)^-}\left\{(\tilde{p}^*)^-(r)-\left(a_n^j\right)^*\frac{Q^*\mu^*(r)}{2r^*}\right\}$$
$$=\frac{T_j^*}{12}\frac{\left(a_n^j\right)^*+\frac{\partial^2(a_n^j)^*}{\partial\theta^2}}{(R_j^*)^2}. \tag{A51}$$

We drop the stars in Eqs. (A50) and (A51) for convenience and arrive at the dimensionless linearized kinematic and dynamic interface conditions:

$$\frac{\partial a_n^j}{\partial t}=\tilde{u}_r(R_j)-a_n^j\frac{Q}{2R_j^2}, \tag{A52}$$

$$\lim_{r\to R_j^+}\left\{\tilde{p}^+(r)-a_n^j\frac{Q\mu(r)}{2r}\right\}-\lim_{r\to R_j^-}\left\{\tilde{p}^-(r)-a_n^j\frac{Q\mu(r)}{2r}\right\}=\frac{T_j}{12}\frac{a_n^j+\frac{\partial^2a_n^j}{\partial\theta^2}}{R_j^2}. \tag{A53}$$

[1] P. Daripa and G. Pasa, An optimal viscosity profile in enhanced oil recovery by polymer flooding, Int. J. Eng. Sci. **42**, 2029 (2004).

[2] *Enhanced Oil Recovery*, edited by F. Fayers (Elsevier, Amsterdam, 1981), p. 596.

[3] G. Pope, The application of fractional flow theory to enhanced oil-recovery, Soc. Pet. Eng. J. **20**, 191 (1980).

[4] *Improved Oil Recovery by Surfactants and Polymer Flooding*, edited by D. Shah and R. Schechter (Academic Press, New York, 1977), p. 513.

[5] R. L. Slobod and J. S. Lestz, Use of a graded viscosity zone to reduce fingering in miscible phase displacements, Prod. Mon. **24**, 12 (1960).

[6] P. Daripa and C. Gin, Studies on dispersive stabilization of porous media flows, Phys. Fluids **28**, 082105 (2016).

[7] G. Homsy, Viscous fingering in porous media, Annu. Rev. Fluid Mech. **19**, 271 (1987).

[8] P. Saffman and G. Taylor, The penetration of a fluid into a porous medium or Hele-Shaw cell containing a more viscous liquid, Proc. R. Soc. London Ser. A **245**, 312 (1958).

[9] J. Bataille, Stability of a radial immiscible drive, Rev. Inst. Pétrole **23**, 1349 (1968).

[10] S. Wilson, Measurement of dynamic contact angles, J. Colloid Interface Sci. **51**, 532 (1975).
[11] L. Paterson, Radial fingering in a Hele–Shaw cell, J. Fluid Mech. **113**, 513 (1981).
[12] H. Zhao, J. Casademunt, C. Yeung, and J.V. Maher, Perturbing Hele–Shaw flow with a small gap gradient, Phys. Rev. A **45**, 2455 (1992).
[13] E. Dias and J. Miranda, Finger tip behavior in small gap gradient Hele-Shaw flows, Phys. Rev. E **82**, 056319 (2010).
[14] T. Al-Housseiny, P. Tsai, and H. Stone, Control of interfacial instabilities using flow geometry, Nat. Phys. **8**, 747 (2010).
[15] T. Al-Housseiny and H. Stone, Controlling viscous fingering in tapered Hele-Shaw cells, Phys. Fluids **25**, 092102 (2013).
[16] D. Lu, F. Municchi, and I. Christov, Computational analysis of interfacial dynamics in angled Hele-Shaw cells: Instability regimes, Transp. Porous Media **131**, 907 (2020).
[17] S. Jackson, H. Power, D. Giddings, and D. Stevens, The stability of immiscible viscous fingering in Hele-Shaw cells with spatially varying permeability, Comput. Methods Appl. Mech. Eng. **320**, 606 (2017).
[18] P. Anjos, E. Dias, and J. Miranda, Fingering instability transition in radially tapered Hele-Shaw cells: Insights at the onset of nonlinear effects, Phys. Rev. Fluids **3**, 124004 (2018).
[19] G. Bongrand and P. Tsai, Manipulation of viscous fingering in a radially tapered cell geometry, Phys. Rev. E **97**, 061101(R) (2018).
[20] L. Morrow, T. Moroney, and S. McCue, Numerical investigation of controlling interfacial instabilities in non-standard Hele-Shaw configurations, J. Fluid Mech. **877**, 1063 (2019).
[21] L. Schwartz, Instability and fingering in a rotating Hele–Shaw cell or porous medium, Phys. Fluids A **1**, 167 (1989).
[22] L. Carrillo, F. X. Magdaleno, J. Casademunt, and J. Ortin, Experiments in a rotating Hele–Shaw cell, Phys. Rev. E **54**, 6260 (1996).
[23] E. Alvarez-Lacalle, J. Ortín, and J. Casademunt, Low viscosity contrast fingering in a rotating hele-shaw cell, Phys. Fluids **16**, 908 (2004).
[24] P. Anjos, V. Alvarez, E. Dias, and J. Miranda, Rotating Hele-Shaw cell with a time-dependent angular velocity, Phys. Rev. Fluids **2**, 124003 (2017).
[25] T. Al-Housseiny, I. Christov, and H. Stone, Two-phase fluid displacement and interfacial instabilities under elastic membranes, Phys. Rev. Lett. **111**, 034502 (2013).
[26] J. Lister, G. Peng, and J. Neufeld, Viscous control of peeling an elastic sheet by bending and pulling, Phys. Rev. Lett. **111**, 154501 (2013).
[27] D. Pihler-Puzovic, R. Périllat, M. Russell, A. Juel, and M. Heil, Modelling the suppression of viscous fingering in elastic-walled Hele-Shaw cells, J. Fluid Mech. **731**, 162 (2013).
[28] D. Pihler-Puzovic, A. Juel, and M. Heil, The interaction between viscous fingering and wrinkling in elastic-walled Hele-Shaw cells, Phys. Fluids **26**, 022102 (2014).
[29] D. Pihler-Puzovic, G. Peng, J. Lister, M. Heil, and A. Juel, Viscous fingering in a radial elastic-walled Hele-Shaw cell, J. Fluid Mech. **849**, 163 (2018).
[30] E. Dias and J. Miranda, Determining the number of fingers in the lifting Hele-Shaw problem, Phys. Rev. E **88**, 043002 (2013).
[31] Z. Zheng, H. Kim, and H. Stone, Controlling viscous fingering using time-dependent strategies, Phys. Rev. Lett. **115**, 174501 (2015).
[32] C. Vaquero-Stainer, M. Heil, A. Juel, and D. Pihler-Puzović, Self-similar and disordered front propagation in a radial Hele-Shaw channel with time-varying cell depth, Phys. Rev. Fluids **4**, 064002 (2019).
[33] S. Gorell and G. Homsy, A theory of the optimal policy of oil recovery by the secondary displacement process, SIAM J. Appl. Math. **43**, 79 (1983).
[34] P. Daripa and G. Pasa, A simple derivation of an upper bound in the presence of a viscosity gradient in three-layer Hele-Shaw flows, J. Stat. Mech. Theory Exp. (2006) P01014.
[35] P. Daripa, Some useful upper bounds for the selection of optimal profiles, Physica A **391**, 4065 (2012).
[36] A. He, J. Lowengrub, and A. Belmonte, Modeling an elastic fingering instability in a reactive Hele-Shaw flow, SIAM J. Appl. Math. **72**, 842 (2012).
[37] P. Coussot, Saffman-Taylor instability in yield-stress fluids, J. Fluid Mech. **380**, 363 (1999).

[38] J. Fontana, E. Dias, and J. Miranda, Controlling and minimizing fingering instabilities in non-Newtonian fluids, Phys. Rev. E **89**, 013016 (2014).
[39] H. Thomé, M. Rabaud, V. Hakim, and Y. Couder, The Saffman–Taylor instability—from the linear to the circular geometry, Phys. Fluids A **1**, 224 (1989).
[40] E. Brener, D. Kessler, H. Levine, and W.-J. Rappel, Selection of the viscous finger in the 90° geometry, Europhys. Lett. **13**, 161 (1990).
[41] M. Ben Amar, V. Hakim, M. Mashaal, and Y. Couder, Self-dilating viscous fingers in wedge-shaped Hele–Shaw cells, Phys. Fluids A **3**, 1687 (1991).
[42] R. Combescot and M. Ben Amar, Selection of Saffman–Taylor fingers in the sector geometry, Phys. Rev. Lett. **67**, 453 (1991).
[43] S. Li, J. Lowengrub, J. Fontana, and P. Palffy-Muhoray, Control of viscous fingering patterns in a radial Hele-Shaw cell, Phys. Rev. Lett. **102**, 174501 (2009).
[44] C.-Y. Chen, C.-W. Huang, L.-C. Wang, and J. Miranda, Controlling radial fingering patterns in miscible confined flows, Phys. Rev. E **82**, 056308 (2010).
[45] C.-Y. Chen and E. Meiburg, Miscible porous media displacements in the quarter five-spot configuration. Part 1. The homogeneous case, J. Fluid Mech. **371**, 233 (1998).
[46] Q. Yuan and J. Azaiez, Miscible displacements in porous media with time-dependent injection velocities, Transp. Porous Media **104**, 57 (2014).
[47] E. Dias, F. Parisio, and J. Miranda, Suppression of viscous fluid fingering: A piecewise-constant injection process, Phys. Rev. E **82**, 067301 (2010).
[48] E. Dias, E. Alvarez-Lacalle, M. Carvalho, and J. Miranda, Minimization of viscous fluid fingering: A variational scheme for optimal flow rates, Phys. Rev. Lett. **109**, 144502 (2012).
[49] Y. Huang and C. Chen, A numerical study on radial Hele-Shaw flow: Influence of fluid miscibility and injection scheme, Comput. Mech. **55**, 407 (2015).
[50] T. Beeson-Jones and A. Woods, On the selection of viscosity to suppress the Saffman-Taylor instability in a radially spreading annulus, J. Fluid Mech. **782**, 127 (2015).
[51] P. Daripa, Studies on stability in three-layer Hele-Shaw flows, Phys. Fluids **20**, 112101 (2008).
[52] P. Daripa, Hydrodynamic stability of multi-layer Hele-Shaw flows, J. Stat. Mech. Theory Exp. (2008) P12005.
[53] S. Cardoso and A. Woods, The formation of drops through viscous instability, J. Fluid Mech. **289**, 351 (1995).
[54] T. Ward and A. White, Gas-driven displacement of a liquid in a partially filled radial Hele-Shaw cell, Phys. Rev. E **83**, 046316 (2011).
[55] A. White and T. Ward, Constant pressure gas-driven displacement of a shear-thinning liquid in a partially filled radial Hele-Shaw cell: Thin films, bursting and instability, J. Non-Newtonian Fluid Mech. **206**, 18 (2014).
[56] C. Gin and P. Daripa, Stability results for multi-layer radial Hele-Shaw and porous media flows, Phys. Fluids **27**, 012101 (2015).
[57] P. Anjos and S. Li, Weakly nonlinear analysis of the Saffman–Taylor problem in a radially spreading fluid annulus, Phys. Rev. Fluids **5**, 054002 (2020).
[58] M. Zhao, P. Anjos, J. Lowengrub, and S. Li, Pattern formation of the three-layer Saffman–Taylor problem in a radial Hele-Shaw cell, Phys. Rev. Fluids **5**, 124005 (2020).
[59] E. Dias and J. Miranda, Taper-induced control of viscous fingering in variable-gap Hele-Shaw flows, Phys. Rev. E **87**, 053015 (2013).
[60] H. Darcy, *Les Fontaines Publiques de la Ville de Dijon* (Dalmont, Paris, 1856).
[61] C. Park and G. Homsy, Two-phase displacement in Hele–Shaw cells: Theory, J. Fluid Mech. **139**, 291 (1984).